UNIVERSITY OF CALIFORNIA,

IRVINE

Sensitivity of response of skewed bridges to their span length, number of bents and abutment modeling

THESIS

Submitted in partial satisfaction of the requirement
for the degree of

MASTER OF SCIENCE

in Civil Engineering

by

Shayan Sheikhakbari

Thesis Committee:
Associate Professor Farzin Zareian, Chair
Adjunct Professor Farzad Naeim
Professor Lizhi Sun

2016

DEDICATION

To

My parents and my brother

In recognition of their worth

Table of Contents

Table of Figures

Table of Tables

ACKNOWLEDGMENT

I would like to express my deepest appreciation to my advisor , Professor Farzin Zareian, you have been a tremendous mentor for me. I would like to thank you for believing in me, encouraging my research, and for allowing me to grow. Your advice on research has been priceless. I could not have imagined better advisor and mentor for my master's study. I would also like to thank my committee members, Adjunct Professor Farzad Naeim, and Professor Lizhi Sun for serving as my committee members and for their supports towards the successful completion of this research.

I would also like to thank Dr.Anoosh Shamsabadi whose vast knowledge in the area of geotechnical engineering provided direction and a source of inspiration. I am extremely grateful for your assistance and suggestions throughout my project.

These acknowledgements would not be completed without mentioning my research colleagues of Performance Based Earthquake Engineering Lab to share knowledgeable discussion and joy, including Dr.Behzad Zakeri, Dr.Bahareh Mobasher, Marta De Bortoli, Lohrasb Keykhosropour.

ABSTRACT OF THE THESIS

Sensitivity of response of skewed bridges to their span length, number of bents and abutment modeling

By

Shayan Sheikhakbari

Master of Science in Civil Engineering

University of California, Irvine, 2016

Associate Professor Farzin Zareian, Chair

Sensitivity of the seismic performance of two typical bridges to the modeling variation of their abutment parameters is investigated and compared through a comparison parameter proposed in this study. One of the bridges is a two-span two-column-bent bridge with seat-type skew abutment and the other is a three-span three-column-bent bridge with seat-type skew abutment. A set of 40 pulse-like ground motions is applied to the bridges for nonlinear time-history analysis.

In the transverse direction, two force-deformation models, which are based on strut-and-tie and sliding shear friction mechanisms, are used. The analytical models are based on the extensive experimental research previously conducted.

A hyperbolic force-deformation model (General Hyperbolic Force Deformation) is used to represent the passive lateral resistance of the abutment backfill. For considering the possible

variation in the backfill geotechnical property, three typical abutment backfill is chosen from the exciting data that was collected from multiple highway bridges in California. Two alternative methods are used to account for the effect of the abutment skew angle on the backfill reaction. The methods include an empirical relationship derived from experimental data, and an analytical method developed based on assumed log-spiral soil failure mechanism.

A comparison parameter is proposed in this study, which is a representative of ductility demand of a skewed bridge to the same non-skewed bridge. For each case, the parameter is computed using the data derived from the nonlinear time-history analysis to investigate the seismic performance of bridges and compare the ductility demand of the specimen bridges.

The outcome of this research reveals the significance of shear keys and abutment backfill on the global response of bridges. The sensitivity of the comparison parameter to the specimen bridges' geometry is also discussed in detail in this study.

Chapter 1

INTRODUCTION

1.1 Problem Description

Skewed reinforced concrete box girder bridges, bridges with skewed-angled abutments, are regularly used as waterway or roadway overcrossing, especially in highway intersections and crowded metropolitan areas where the inadequacy of space makes the use of skew geometry necessary. The investigation of previous earthquakes damage to bridges has shown that the differences between the responses of skewed and straight bridges are significant.(EERI, 1991; EERI, 1995; Iwasaki et al. 1972; Jennings et al., 1971; Kawashima et al.,2010; Yashinsky et al., 2010). The main difference is that the skewed bridges suffer more from an in-plane offset at the abutment because of their tendency to rotate about their vertical axis during an earthquake. Based on the 2010 National Bridge Inventory (NBI) (FHWA Bridge Program NBI Data, 2010) records, 60 percent of the bridges in California are skewed. The data shows the importance of seismic performance assessment of skewed bridges.

During the past decade, the focus of engineering research has been on investigating the seismic response of skewed bridges subjected to ground motions aiming at proposing recommendations for more reliable seismic design of these structures. To analyze the behavior of skewed bridges, analytical models were created with different assumptions resulting in inconsistent seismic performance (Goel and Chopra, 1997; Wakefield et al., 1991). Implementation of a more realistic modeling technique is necessary for the numerical simulation to capture a more accurate response of existing skewed bridges in a nonlinear regime. To aim this, more experimental and analytical studies are required to create and examine skewed abutment models.

1.2 Objectives and Scope

The primary objective of this research is to assess the performance of a multi-span bridge and to compare it with that of a two-span bridge. The behavior of the exterior shear keys and the abutment backfill has a significant impact on the response of the skewed bridges, therefore, more attention is dedicated to the abutment modeling techniques. Moreover, a modeling method is recommended for the modeling of the cap beam for 3-column bent bridges simulated by a spine-line model. In this study, two built-in concrete box girder bridges in California with seat-type abutments are used. For the nonlinear analysis, 40 pulse-like ground motions representing the types of expected seismic excitation in California are used. The IM-EDP response trends are obtained by nonlinear time history analyses using aforestated ground motions to compare the performance of different bridges.

1.3 Literature Review

In recent years, thanks to extensive exterior shear keys and abutment backfill soil experiments, the development of reliable analytical models that represent a realistic as-built abutment behavior has become possible. In the following, a succinct review of the experiments and the research projects carried out pertinent to the development the analytical models used in this study is provided.

1.3.1 Exterior Shear Key

Exterior shear keys have a significant effect on the bridge response in a seismic event. Shear keys are mostly used in bridges with seat-type abutment where there is more control over the seismic force quantity against which it can resist. The structure of a seat-type abutment permits the superstructure to move more independently from the abutment. The seat-type abutment,

however, has a higher possibility of failing because of superstructure rotation or unseating when the abutment has skew angle. Within this setting, exterior shear keys act as structural fuses. They have limited resistance to restrain the superstructure from rotating and transfer the lateral loads to the stem wall and the piles of the abutment. The capacity of a sacrificial exterior shear key should be limited to the level that its failure occurs before it overloads the piles and the stem wall. The diagonal cracks observed on the abutment stem walls in some bridges subjected to previous earthquakes, such as Northridge 1994 and Chile 2010, imply the ductile behavior for the exterior shear keys despite the fact that that they are designed to be sacrificial elements.

The studies carried out on the behavior of the shear keys identified two types of failure modes for the exterior shear key joints (Henson et al. 1961; Buyukozturk et al.1990; Kaneko and Li 1993; Silva et al 2003): (1) a single horizontal crack that develops at the interface (Sliding Shear Mechanism), (2) multiple diagonal cracks along the direction of predominant principal compressive stresses (Diagonal Tension Mechanism). Some shear friction models were developed for the first mechanism after extensive experiments on the performance of the reinforced concrete section of shear keys (Anderson 1960; Mast 1968; Mattock and Hawkins 1972; Mattock 1974; Paulay et al. 1974; Mattock 1975; Mattock 1981; Walraven et al. 1987; Tassios and Vintzeleeou 1987). In this research, the model suggested by the Caltrans Bridge Design Specification is used.

New criteria for design of shear keys emerged after the 1994 Northridge earthquake. Subsequently, engineers rushed to investigate the efficiency of the new criteria for design of shear keys. Bozorgzadeh et al. (2004) and Megally et al. (2001) conducted an extensive experimental research on the behavior of different types of shear keys at UCSD in 2001. A total of 5 specimens (10 shear keys) were built at the 40% scale of the exterior shear keys of a

prototype abutment. The specimens were subjected to various cyclic loads to determine the maximum capacity of the shear keys and the required reinforcement ratio to reach to a specific capacity. Furthermore, it was investigated if the shear keys designed by the new Caltrans specifications were behaving as sacrificial elements. They identified that the failure mechanism was dependent on the following factors: 1) the construction joint types between the shear key and the abutment stem wall, 2) the amount and configuration of the vertical reinforcement crossing the shear key interface and the abutment stem wall, and 3) the configuration of the horizontal reinforcement in the stem wall. An analytical model was developed to simulate the behavior of the exterior shear key for the second type of failure mechanism as a result of the experimental program. The model was used in many studies for simulating the exterior shear key element.(Aviram et al., 2008; Goel and Chopra 2008; Kaviani et al. 2012).

Aviram et al. (2008) developed practical guidelines for the modeling and nonlinear analysis of bridge structures to assist university researchers and practicing engineers in the implementation of nonlinear methods. In the proposed guidelines, the model suggested for the exterior shear key was derived from the experimental research of Megally et al. 2002. The sliding shear friction model was chosen for the shear keys and its ultimate strength was assumed to be 30% of the superstructure dead load vertical reaction at the abutment according to the SDC 2004.

Goel and Chopra (2008) used three different shear-key conditions to investigate the role of shear keys on the seismic behavior of ordinary bridges: 1) the idealized analytical strut-and-tie shear key model reported by Bozorgzadeh et al. (2006), 2) elastic shear key which does not shear off and keep providing transverse restraint all through a ground motion, and 3) no shear key. It was concluded that even though upper bound values of column drift and deck displacement can be estimated by the analysis of elastic shear keys and no shear keys respectively, nonlinear force-

deformation relationship of shear keys have to be considered to determine the seismic demand accurately. The first complication of nonlinear modeling of the shear keys is the underestimation of seismic demands if they happen to be modeled with more strength for which they were designed. Secondly, a nonlinear response history analysis of a bridge structure is required if the nonlinear shear key model is chosen.

Two types of reinforcing details for shear keys are provided in the Caltrans Seismic Design Criteria (SDC 1.7): 1) isolated shear key based on the experimental tests of Bozorgzadeh et al. (2007), and 2) non-isolated shear key based on the shear friction provisions of LRFD BDS. Amongst the exterior shear key test units in the experimental study by Bozorgzadeh et al. (2007), the design and the construction details of two specimens were provided by Caltrans. In spite of a shear sliding failure that was expected from loading the sacrificial exterior shear keys, a large diagonal crack was developed in the stem wall of the two test units. The crack in the stem wall rather than at the interface of the abutment stem wall-shear key contradicts with the assumption that a shear key designed by Caltrans acts as a structural fuse. Several recommendations were proposed for the constructions details of sacrificial shear keys in the experimental study to solve the problem.

1.3.2 Backfill Passive Resistance of Abutment

The seismic design of bridges is based on a displacement performance philosophy using nonlinear static pushover analysis. Therefore, the soil resistance of abutment backfill is necessary to be predicted for such a bridge design philosophy. The studies which have been carried out to investigate the effects of different aspects of abutment modeling on the seismic response of bridges can be categorized into two main types. One category focuses on the interaction between the superstructure and the abutment components of a bridge (shear keys, bearing pads, and pile

foundation) while considering the boundary conditions such as backfill response and the pounding effect. The other category aims its attention at developing constitutive analytical models which define the force-deformation behavior of various abutment components from large-scale experimental data and advanced finite element simulations.

Shamsabadi et al. (2004) investigated the effect of ground motions with various amplitudes of velocity pulses on a three-span skewed bridge. A three-dimensional finite element model was created using the computer program SAP2000 with a more focus on the simulation of the nonlinear dynamic soil-abutment-structure interaction of the skewed bridge. For complete representation of the longitudinal backfill soil-structure interaction with the bridge deck, the abutment model consists of an expansion gap, a near-field, and a far-field effect. The gap element representing the expansion gap is connected to the bridge deck and placed in series to a nonlinear spring accounting for the passive response of the abutment. The gap and the nonlinear spring system are included in series with the element representing the far-field effect. The far-field effect is modeled with an elastic spring connected to radiation damping dashpot in parallel. The effects of the shear keys and backwall participation in the transverse and the longitudinal direction are not considered respectively in the study.

Three types of abutment models are proposed by Aviram et al. (2008) with different levels of complexity and their effects are investigated on the overall seismic response of six bridges in the study. The simplest model is the roller abutment which consists of single supporting points constraining the abutment against the displacement in the vertical directions. The model can be used to estimate the lower-bound longitudinal and transverse abutment resistance. Another proposed model is the simplified abutment and consists of a rigid element which is attached to the superstructure and has the length of the superstructure width. The longitudinal, transverse

and vertical nonlinear response are all defined at each end of the rigid element. Accounting for the response of the longitudinal backfill soil, a zero-length element is used with assigned elastic-perfectly-plastic backbone curve (as suggested by SDC section 7.8.1). The vertical direction is defined by an elastic spring with the stiffness equivalent to that of the bearing pad stiffness. The spring abutment is the most complex model and has sophisticated longitudinal, transverse, and vertical nonlinear abutment response. A lumped mass is also used in the spring abutment model representing the concrete abutment and the mobilized embankment soil participation. Based on the results of the study, implementation of the roller abutment model is appropriate for the simulation of long-span bridges since the abutment behavior does not govern their global response. The simplified abutment model does not have enough detail to represent the realistic transverse response of a bridge, even though it is suitable enough to estimate the longitudinal response of a bridge.

Huo (2011) calibrated the longitudinal and transverse p-y springs for different soil properties and abutment wall height by modeling a 3D finite element abutment. Accounted for the longitudinal gap and the soil friction between the backwall and the backfill, the p-y springs were coupled with a contact-friction element assigned with a pressure dependent friction capacity in the transverse direction and no tension capacity in the longitudinal direction. For considering the effects of the pounding impact, elastomeric bearings, and the embankment impedance, Huo and Zhang (2012) used gap element, elastoplastic and contact linear springs in addition to the equivalent linear spring and viscous dashpots recommended by Zhang and Makris(2002) for the models.

1.3.3 Bridges with Skew Abutments

The damage investigation of the bridges collapsed due to the Northridge 1994 and Chile 2010 earthquakes (Buckle, I. G. 1994, Kawashima, K .et al. 2011) has drawn researcher’s attention to

the seismic performance of skewed bridges. Insufficient insight into the seismic effects on the skewed bridges resulted in an extensive damage caused by the earthquakes. Based on the results of a large-scale field test (Marsh et al. 2013) and an experimental research (Rollins et al. 2012) after the disasters, increasing the skew angle of an abutment decreases the backfill passive resistance force significantly.

Three seismic response parameter were considered for developing IM-EDP curves: maximum column bent drift ratio, maximum abutment unseating displacement, maximum planar deck rotation.

Shamsabadi and Kapuskar (Shamsabadi et al. 2006) developed three-dimensional finite-element models of five bridges with various span lengths and bent configuration to evaluate the seismic response of the abutments to near-source ground motions as a function of the skew angle. Using nonlinear analyses, an intense increase in the amount of deck rotation can be observed shortly after the velocity pulse is applied to the bridge during the initial cycles causing the deck to become unseated at the abutment or resulting in a permanent residual rotation. Furthermore, it can be concluded that high rigidity of the bridge structure results in reduction of deck rotation. The critical role of the shear keys in controlling and complication of the global bridge response is also shown in the results. Finally, the nonlinear analysis of the three-dimensional model of bridges with high abutment skew angle was recommended for better understanding the behavior of the structure.

Kaviani et al. (2012) conducted extensive research on the behavior of the skewed bridges and provided valuable recommendations for practicing engineers for their design. His works included proposing a novel skewed bridge modeling techniques that help to create models representing

their realistic seismic behavior and assessing the seismic response of skewed bridges by sensitivity analysis of bridge response parameters. They modeled the shear keys using the strut-and-tie method and concluded that the shear keys have a significant effect on the behavior of the skewed bridges. The effect was noticeable on EDPs such as abutment unseating, and column drift ratio.

Zakeri et al. (2013) conducted research on the sensitivity of single-frame box girder types of bridges to the abutment skew angle considering different seismic detailing of the bridge, type of abutment (i.e., integral or seat-type), number of columns in each bent (i.e., single- or two-column bents). The abutment modeling details were inconsistent with the approaches recommended by Aviram et al. (2008), Nilson and DesRoches (2006) and Nilson (2005). The results of their study reveal that the abutment skew angle has a significant effect on the seismic response of post-1994 single-frame bridges with seat-type abutment.

Chapter 2

Analytical Models and Analysis Methods

2.1 Overview

In this chapter, the methodology used to model two skewed abutment specimen bridges is presented. The implemented modeling techniques were mainly based on the recommendations of Caltrans Seismic Design Criteria (2013) and the research conductivity Aviram et al. (2008). Since the primary purpose of the study is to assess the behavior of skewed bridges, more focus was placed on the techniques used for the skewed abutment modeling, which is described in his chapter thoroughly.

The bridges are modeled by two nonlinear analytical programs, SAP 2000 (CSI, 2014), and OpenSees (McKenna et al., 2000). The orientation of our discussion is toward the OpenSees modeling approach. The models created by SAP 2000 were mainly for validating some OpenSees modeling methods and parameters.

In this study, OpenSees(version 2.4.4) nonlinear finite element software (McKenna et al., 2000) is used to simulate the response of the bridges and the abutment backfill systems subjected to pulse-like ground motions. The framework facilitates numerical modeling for earthquake engineering applications by providing adequate libraries of materials, elements, and analysis commands. Its platform makes multiple executions of a scripted block of code possible while model variables and ground motion time histories can be changed.

2.1.1 Selected Bridges for This Research

Two specimen bridges are used in this study. The first bridge, Bridge B, is the La Veta Avenue Overcrossing located in the city of Tustin, California. Its superstructure is a six-cell continuous reinforced concrete box girder, and it has a two reinforced concrete circular columns. The second bridge, Bridge C, is the Jack Tone Road Overhead located in the city Ripon, California. The bridge has a seven-cell continuous reinforced concrete box girder superstructure and two three-column bents. Figure 2-1 and Figure 2-2 show the bridges in elevation.

Bridge B has straight seat-type abutments. Although the abutment of Bridge C is high cantilever type, it is modeled as a seat type abutment to be comparable to the other bridge. In Table 2-1 and Table 2-2, the major geometrical and structural aspects of the selected bridges are discussed.

2.2 Material Properties and Modeling

The material properties are appointed from the Caltrans Seismic Design Criteria (2013). The Mander's stress-strain model (Mander et al., 1988) was used for the stress-strain relationship of confined and unconfined concrete (Figure 2-3).The parameters used to create the model are as followed:

ε_{c0} = 0.0028, f'_{ce}= 34.5 MPa, ε_{sp}= 0.005 (for unconfined concrete)

ε_{cc}= 0.008, f'_{cc}= 45.0 MPa, ε_{cu}= 0.025 (for unconfined concrete)

$$E_c = 0.043 \times w^{1.5} \times \sqrt{f'_c} \quad \text{(Based on Caltrans SDC 2013)} \qquad (2-1)$$

where:
ε_{c0}: Strain corresponding to maximum unconfined concrete
ε_{sp}: Maximum unconfined concrete strain
ε_{cc}:Strain corresponding to maximum confined concrete
ε_{cu}: The ultimate compressive strain of confined concrete where the first hoop fractures
f'_{ce}: Unconfined concrete strength
f'_{cc}: Maximum confined concrete strength

f'_c:Compressive strength of unconfined concrete (34.5 MPa)
w: unit weight of concrete
E_c: Concrete modulus of elasticity

For the reinforcing steel material, A706/A706M was used, with the steel modulus of elasticity of E_S = 200000 MPa and the expected yield strength of f_{ye}= 475 MPa based on the Caltrans SDC (2013).

In the following, the material models which were employed from the rich collection of Opensees models are briefly explained.

Concrete01: a uniaxial Kent-Scott-Park concrete material object with degraded linear unloading/reloading stiffness according to the work of Karsan-Jirsa and no tensile strength. (Opensees Wiki) Figure 2.4 (a)

Conctrete02: a uniaxial concrete material object with tensile strength and linear tension softening. (Opensees Wiki) Figure 2.4 (b)

ReinforcingSteel : a uniaxial material which is intended to be used in a reinforcing concrete fiber section as the steel reinforcing material. The backbone curve is shifted as described by Chang and Mander (1994) to account for Isotropic hardening.(Opensees Wiki) Figure 2.5

Hysteretic: a uniaxial bilinear hysteretic material object with pinching of force and deformation, damage due to ductility and energy, and degraded unloading stiffness based on ductility. (Opensees Wiki)

2.3 Component Modeling

A three-dimensional spine-line model of each bridge was simulated with the line elements at the centroid of the cross sections of each component of the bridge. The models consist of superstructure, column-bents, expansion joints, shear keys and abutments. A representative 3-D analytical bridge model which was used in this study is shown schematically in Figure 2.6.

Previous research proved that the global response of short bridges is significantly dependent on the modeling assumptions.(Kaviani et al., 2011; Priestley et al., 1996).

To capture the response of skewed bridges, their models incorporate components including the abutment transverse and longitudinal springs, abutment gap and column plastic hinge with nonlinear behavior. The pile cap connection to the column bents is considered pinned for both of the specimen bridges. In the following, the main modeling assumptions of each component are enumerated.

2.3.1 Deck Modeling

To simplify the numerical modeling, the superstructure is simulated as an elastic component using elastic beam-column elements. The main reason for using elastic element is that flexural yielding of the deck is not expected during a seismic event.

The value of the effective moment of inertia for the reinforced concrete box girder, denoted as I_{eff}, is between 0.5 I_g- 0.75 I_g, with the upper bound and lower bound values representing the heavily reinforced section and lightly reinforced section respectively. The value of I_{eff} depends on the extent of cracking in the cross section. However, no stiffness reduction is recommended by SDC (2013) since stiffness variation as the result of moment reversal cannot be captured in a multi modal elastic analysis. The SAP-2000 model of each bridge was used to calculate the moments of inertia of the deck cross section in both directions.

To distribute the superstructure load in the Opensess model, a node and a lumped mass with a value based on tributary length is assigned at every one tenth length of each. The rotational mass of the superstructure is also assigned to deck nodes aiming at identifying bridge fundamental modes more accurately. The rotational moment of inertia of each superstructure segment is calculated as follows:

$$M_{xx} = \frac{M{d_w}^2}{12} = \frac{(m/L)L_{trib}\,{d_w}^2}{12} \qquad (2-2)$$

Where:

M_{xx} : The rotational mass of the superstructure.

M : The total mass of the superstructure segment

m/L : Mass of the superstructure per length

L_{trib} : Length of the superstructure

d_w : The superstructure width

2.3.2 Cap Beam Modeling

An elastic frame element was used to represent each cap beam. The modeled cap beam has a rectangular cross section with dimensions based on the geometry of the bridge. Since the cap beam and the superstructure are generally constructed monolithically, the connection of the cap beam to the superstructure is modeled as fully constrained. The cap beam is expected to remain rigid and not to have any bending in the plane of the structure in spite of its out of plane behavior. Furthermore, the dimensions of the part the superstructure-cap beam system that is resisting torsion is much greater than that of cap beam's cross section. Therefore, the moment of inertia in the plane of the superstructure and the torsional constant of the cap beam's cross section are magnified ($\times 10^5$). To correctly model the cap beam-deck connection in bridge C, the deck element is connected to a completely rigid element parallel to the cap beam and then the rigid element is attached to the cap beam with few rigid springs on each side of the cap beam. To evaluate the validity of the model, a simple SAP 2000 model of bridge C was simulated with the superstructure modeled with a thin shell element. The cap beam model of Bridge C is depicted in Figure 2.7.

2.3.3 Column-Bent Modeling

Inelastic three-dimensional beam-column elements are used to represent behavior of columns. The *UniaxialMaterial* tag was assigned to the column's fiber sections from Opensees modeling collection (Figure 2.8).

At each end of the column, plastic hinges can be developed near the point of fixity. From the point of inflection to the point of fixity, the column curvature increases linearly. Caltrans SDC(2013) proposed an analytical equation to calculate the plastic hinge length in a column:

$$L_P = \begin{cases} 0.08L + 0.15f_{ye}d_{bl} \geq 0.3f_{ye}d_{bl} & (in, ksi) \\ 0.08L + 0.022f_{ye}d_{bl} \geq 0.044f_{ye}d_{bl} & (mm, MPa) \end{cases} \qquad (2-3)$$

Where :

L : Column height

f_{ye} : Expected yield stress for A706 reinforcement

d_{bl} : The nominal bar diameter of the longitudinal diameter

To achieve the dynamic response and the bridge fundamental modes more accurately, rotational mass of columns are considered in the model. The rotational moment of inertia of each column segment is calculated as follows:

$$M_{zz} = \frac{MR_{col}{}^2}{2} = \frac{(m/L)L_{trib}\,D_{col}{}^2}{8} \qquad (2-4)$$

Where:

M_{zz} : The rotational mass of the column.

M : The total mass of the column segment

m/L : Mass of the column per length

L_{trib} : The tributary length

R_{col} : The radius of the column

D_{col} : The diameter of the column

2.3.4 Abutment Modeling

A large body of analytical and experimental research has been conducted on deriving a realistic model for bridge abutments (Aviram et al. 2008; Bozorgzadeh et al. 2006; Bozorgzadeh et al. 2008; Goel and Chopra, 1997; Shamsabadi et al., 2007; Shamsabadi et al. 2010; Wilson and Tan, 1990; Kaviani et al., 2012). In this study, the bridge abutments are modeled based on Spring Abutment model suggested by Aviram et al. (2008). However, the force-deformation relationship assigned to the springs in this research is taken from more recent studies. The springs used to model the behavior of the abutment can be categorized into 3 groups: 1) longitudinal response of the backfill passive pressure, 2) the shear keys transverse response 3) the stem wall and the bearing pads vertical response.

2.3.4.1 Longitudinal response

The Generalized Hyperbolic Force-Deformation (GHFD) relationship is used for modeling the backfill passive resistance. GHFD is a simple closed-form relationship for lateral response of abutment backfill which is based on the LSH model proposed by Shamsabadi et al. (2007). For estimating abutment nonlinear force-displacement capacity in LSH model, limit-equilibrium method using mobilized logarithmic-spiral failure surface is coupled with a modified hyperbolic soil stress-strain behavior.

2.3.4.1.1 LSH model (Shamsabadi et al. 2005, Shamsabadi et al. 2007)

A hyperbolic relationship between the deviatoric stress $(\sigma_1 - \sigma_3)$ and the vertical strain ε during triaxial soil test is applied to derive the formulation of the intermediate mobilized passive wedge. In the following, Duncan and Chang (1970) hyperbolic model is used as shown in Figure 2.9.

$$(\sigma_1 - \sigma_3)_i = \frac{\varepsilon_i}{\frac{1}{E_o} + \frac{\varepsilon_i}{(\sigma_1 - \sigma_3)_{ult}}} \qquad (2-5)$$

Where:

$(\sigma_1 - \sigma_3)_i$: Intermediate deviatoric stress

$(\sigma_1 - \sigma_3)_{ult}$: Ultimate deviatoric stress at failure

ε_i : Strain level

E_o : Initial tangent modulus

As it is shown in Figure 2.9 (b), the deviatoric stresses increase to an asymptotic value denoted as the ultimate deviatoric stress. The failure deviatoric stress is defined at which the soil is assumed to fail. The ratio of the failure deviatoric stress to the ultimate deviatoric stress is expressed as the failure ratio R_f:

$$R_f = \frac{(\sigma_1 - \sigma_3)_f}{(\sigma_1 - \sigma_3)_{ult}} \qquad (2-6)$$

The deviatoric stress ratio $SL(\varepsilon_i)$ is formulated by normalizing the stresses to the stress at failure:

$$SL(\varepsilon_i) = \frac{(\sigma_1 - \sigma_3)_i}{(\sigma_1 - \sigma_3)_f} = \frac{\varepsilon_i}{\frac{(\sigma_1 - \sigma_3)_f}{E_o} + R_f \varepsilon_i} \qquad (2-7)$$

Considering the boundary conditions, Shamsabadi et al. (2007) modified the hyperbolic relationship which is as follows (Figure 2.10):

$$SL(\varepsilon_i) = \frac{\varepsilon_i}{A + B\varepsilon_i} \qquad (2-8)$$

$$A = \frac{\varepsilon_f \varepsilon_{50}}{\varepsilon_f - \varepsilon_{50}} \qquad (2-9)$$

$$B = \frac{\varepsilon_f - 2\varepsilon_{50}}{\varepsilon_f - \varepsilon_{50}} \qquad (2-10)$$

Where :

ε_{50} : a parameter can be determined from geotechnical laboratory testing of a sample from the backfill . Its value is a function of confinement, grain shape, grain size distribution and the relative density of sand and is the function of plasticity index and the drained shear strength for clay.

Norris (1997) empirically calculated that the strain at failure ε_f is 31 times larger than ε_{50}.Therefore the relationship can be expressed as follows:

$$\varepsilon_f = \frac{\varepsilon_{50}}{1 + R_f} \qquad (2-11)$$

By considering the abovementioned equation, the modified hyperbolic stress-strain relationship can also be expressed as a function of the R_f, ε_{50}, ε_f :

$$SL(\varepsilon_i) = \frac{\varepsilon_i}{\frac{\varepsilon_{50}}{R_f} + \left(2 - \frac{1}{R_f}\right)\varepsilon_i} \qquad (2-12)$$

The modified relationship can also be expressed in terms of shear strength based on the Mohr – Column failure criterion as the ratio of the incremental deviatoric stress $(\sigma_1 - \sigma_3)_i$ to deviatoric stress at failure$(\sigma_1 - \sigma_3)_f$ (figure 2.9 (b) and 2.10).

$$SL(\phi_i, c_i) = \frac{(\sigma_1 - \sigma_3)_i}{(\sigma_1 - \sigma_3)_f} = \frac{\sigma_3\left[\tan^2\left(45° + \frac{1}{2}\phi_i\right) - 1\right] + 2c_i \tan(45° + \frac{1}{2}\phi_i)}{\sigma_3\left[\tan^2\left(45° + \frac{1}{2}\phi\right) - 1\right] + 2c \tan(45° + \frac{1}{2}\phi)} \qquad (2-13)$$

$$c_i = \frac{c \tan \phi_i}{\tan \phi} \qquad (2-14)$$

Where :

ϕ_i : Intermediate mobilized friction angle of the soil

ϕ : Fully mobilized friction angle of the soil at failure

c_i : Intermediate mobilized cohesion of the soil

c : Fully mobilized cohesion of soil at failure

As a result of an extensive experimental work, James and Bransby (1971) showed the relationship between wall movement and the backfill shear strain and mobilized shear strength. Therefore, an abutment wall loaded monolithically is resisted by the mobilized passive resistance of backfill behind the abutment as a function of relative displacement between the wall and the backfill. At the intermediate level of displacement, the final passive wedge cannot be formed and the shear strength of the backfill cannot be mobilized. Accordingly, to calculate the intermediate mobilized passive force, at each level of displacement, it is assumed that the developed intermediate passive resistance force is forming a mobilized passive wedge (Figure 2.11 (a)). Since each stress-strain level is associated with the soil properties of each assumed intermediate mobilized passive wedge (Figure 2.11 (b)), with the employment of the slicing method, nonlinear abutment-backfill capacity can be formulated.

The equation of mobilized logarithmic-spiral failure surface is specified as follows (Figure 2.12):

$$r_{ij} = r_{il} e^{\theta_{ij} \tan \phi_{ij}} \qquad (2-15)$$

$$\theta_{ij} = \frac{1}{2} \tan^{-1} \frac{2K \tan \delta_{ij}}{K-1} \qquad (2-16)$$

$$K = \frac{A_1 + A_2}{A_3} \qquad (2-17)$$

$$A_1 = 1 + \sin^2 \phi_{ij} + \frac{c_{ij}}{h_{ij}} \sin 2\phi_{ij} \qquad (2-18)$$

$$A_2 = 2(\cos \phi_{ij}) \times \sqrt{\left(\tan \phi_{ij} + \frac{c_{ij}}{\gamma z_{ij}}\right)^2 + \tan^2 \delta_{ij} \left[4\left(\frac{c_{ij}}{\gamma z_{ij}}\right)^2 + 4\frac{c_{ij}}{z_{ij}} \tan \phi_{ij} - 1\right]} \qquad (2-19)$$

$$A_3 = \cos^2 \phi_{ij} + 4 \tan^2 \delta_{ij} \qquad (2-20)$$

Where:

i : Subscript denoting the quantity associated with intermediate mobilized failure surface i

j : Subscript denoting the quantity associated with intermediate mobilized failure surface j

ϕ_{ij} : Intermediate mobilized soil interface friction angle

c_{ij} : Intermediate mobilized resultant cohesion force along failure surface of a slice

h_{ij} : Intermediate mobilized wall height ($h_i = SL(\varepsilon_i).h_{ult}$)

K : Ratio of horizontal to vertical stresses in the slice

The value of the horizontal component tΔE_{ij} , the resultant of the inter-slice forces E_{ij} and $E_{(i+1)j}$ acting at the sides of slice j (Figure 2.12 (b)) can be defined as:

$$\Delta E_{ij} = \frac{W_{ij} \tan(\alpha_{ij} + \phi_{ij}) + c_{ij} L_{ij} \left[\sin \alpha_{ij} \tan(\alpha_{ij} + \phi_{ij}) + \cos \alpha_{ij}\right]}{1 - \tan \delta_{ij} \tan(\alpha_{ij} + \phi_{ij})} \qquad (2-21)$$

The mobilized horizontal passive capacity F_{ih} can be finally calculated from the summation of the ΔE_{ij} forces(Figure 2.12):

$$F_{ih} = \frac{\sum_{j=1}^{n} \Delta E_{ij}}{1 - \tan \delta_{iw} \tan(\alpha_{iw} + \phi_i)} \qquad (2-22)$$

$$\alpha_{iw} = \theta_{i1} + \alpha_{i1} \qquad (2-23)$$

The local horizontal displacement of slice j related to the mobilized failure surface i is expressed as follows:

$$\Delta y_{ij} = \Delta z_{ij} \frac{\gamma_{ij}}{2} = \Delta z_{ij} \frac{1}{2} \varepsilon_{ij}(1+\nu) \sin \alpha_{ij} \qquad (2-24)$$

Where:
ν : Poisson's ratio of the soil
γ_{ij} : Shear strain in the slice

The relationship between shear strain γ and normal strain ε in the soil is shown in Figure 2.13 based on the Mohr circle associated with failure surface:

$$y_i = \sum_{j=1}^{n} \Delta y_{ij} \qquad (2-25)$$

The LSH model is validated with the existing experimental data from various full-scale pile cap and abutment tests (Shamsabadi et al. 2005 and Shamsabadi et al. 2007).

2.3.4.1.2 GHFD model

Khalili Tehrani et al. (2010) proposed a model for lateral response of abutment backwall. The model is denoted as the GHFD model and was developed using an extensive parametric study on validated limit-equilibrium LSH model. The backfill passive lateral force is only dependent on the backfill soil properties and the backwall height in GHFD model and is defined as follows:

$$F(y) = \frac{\frac{1}{\beta}(\eta-1)\alpha y}{\widehat{H} + \frac{1}{\beta}(\eta-2)y} \widehat{H}^n \qquad (2-26)$$

$$\widehat{H} = \frac{H}{H_r} \qquad (2-27)$$

Where:

F : Backfill passive resistance force

y : Backwall deflection

$\widehat{H}$: The ratio of the backwall height H to the reference height H_r which is equal to 1 meter.

The rest of the parameters are defined as follows:

$$\beta = [1703 - 683.4\,(\tan\phi)^{1.23}]\varepsilon_{50} \qquad (2-28)$$

$$\alpha = \begin{cases} [5.62\,(\tan\phi)^2 + 0.53]\gamma + [10.58\,(\tan\phi)^{1.79} + 2.86]c & ,\phi \neq 0,\ c \neq 0 \\ 1.06\gamma[5.62(\tan\phi)^2 + 0.53] & c = 0 \\ 0.5\gamma + 2.63c & \phi \neq 0 \end{cases} \qquad (2-29)$$

$$n = \begin{cases} 2 & c = 0 \\ \dfrac{0.91(\tan\phi)^{1.2} + 1.49}{\sqrt{c}} + 0.9 & c \neq 0 \end{cases} \qquad (2-30)$$

$$\eta = \begin{cases} 15.47 & \phi < 5°,\ c \neq 0 \\ 18.10 - 9.38\sqrt{\tan\phi} & \phi \geq 5°,\ c \neq 0 \\ 14.36 - 7.49\sqrt{\tan\phi} & c = 0 \end{cases} \qquad (2-31)$$

Where:

ϕ : Backfill soil internal friction angle

c : Backfill soil cohesion

γ: The unit weight of the backfill soil

The Generalized Hyperbolic Force-Deformation (GHFD) relationship is used in the Opensees model to develop the backbone curves of the nonlinear soil springs connected perpendicularly to the rigid elements which represent the abutment backwall. Five nonlinear springs in series with gap elements are employed along the abutment to account for the backfill resistance and gap in between the deck and backwall.

In an extensive experimental field investigation on the typical backfill material used behind bridge abutments across the state of California, four categories are defined for California highway bridges (Earth Mechanics, INC. 2005): I) Dense to very dense sand with gravel, II) Medium dense silty sand, some with gravel, III) Medium dense clayey sands, some with gravel, IV) Stiff-hard Clays with fine to coarse-grained sands, some with silts (Table 2.3). The values of soil friction angle ϕ, the soil cohesion c are the average typical properties of the 95% relative compacted soil samples suggested in the Earth Mechanics,INC., 2005 for each backfill category. The total unit weight γ is calculated by substituting the field dry density ρ_d value and the moisture content w value in the following weight-volume relationship:

$$\gamma = (1 + w) \times \rho_d \qquad (2-32)$$

Soil categories I to III are used in this study as they are utilized more than other types. The values of the ε_{50} and R_f are chosen based on Shamsabadi et al., (2007) recommendations, with R_f being assigned 0.96 and ε_{50} being assigned 0.0035 for all soil categories.

The intermediate and ultimate log-spiral failure surfaces are developed based on the LSH model using Equations (2-5) to (2-20) for a foot unit width of a 6.23 ft high backwall for each backfill category (Figure 2.14). The related LSH force-deformation curves are demonstrated on Figure 2-15. The abscissa and the ordinate of each point on the curves in Figure 2-15 correspond to the backwall deflection and the force necessary to mobilize each of the log-spiral failure surfaces shown in the Figure 2-14. As shown in Figure 2-15, GHFD force-deformation curve is in good agreement with the LSH backbone curve for soil category I while GHFD and LSH curves depart from each other to some extent for soil categories II and III as the backwall deformation increases.

2.3.4.1.3 Backfill with non-uniformly reduced GHFD passive resistance

Based on Rollins et al. 2013 large scale laboratory tests and numerical analyses, the backfill passive resistance force significantly decreases by increasing the skew angle of the abutment. To account for the reductions, Omrani et al. (2016) proposed a method to model passive resistance response of the backfill behind the skewed abutments. According to the method, no force reduction is required for the coordinates along the width of the skewed backwall as long as the extent of the backfill perpendicular to the backwall is long enough for mobilization of the ultimate soil failure surface.

Otherwise, if the length of the extent of backfill perpendicular to the skewed backwall is less than the length of the ultimate failure surface at ground level, the backfill passive resistance should be reduced as explained in the following. The reduced-resistance width (W_r), the length over the width of skewed backwall where the passive force needs to be reduced, can be calculated as a function of skew angle α and the length of the ultimate failure surface at ground level L_u (Figure 2-16):

$$W_r = L_u \tan \alpha \qquad (2-33)$$

As shown in the Figure 2-14, since the length of the ultimate failure surface L_u at the ground level for cohesive soil is less than that of granular soil, the reduced-resistance width of backwall W_r with cohesive backfill soil is lesser too in any abutment skew angle. The tributary width of each of the five nonlinear hyperbolic springs used to model the backfill behavior is denoted as W_t. The ratio of W_r to W_t for the assumed arrangement of springs along the abutments can be found in Table 2-4 as the function of abutment skew angle α and soil category for both bridge specimens. Figure 2-17 shows the distribution of backfill passive resistance behind the backwall

for a general case in which the reduced-resistance width exceeds the length of the spring tributary width.

The geometry of backwall in both specimen bridges is very similar including the height and length (Table 2-1 and Table 2-2). Therefore, the values in Table 2-4 can be used for both bridges. The reduced-resistance width of abutments for both bridges at all skew angles and for all backfill categories remains less than the tributary backfill width which is the same for the springs in both bridges because of having the same backwall length ($W_r/W_t \leq 1$). As a result, the backfill passive resistance of the spring which is near the acute corner needs to be reduced. The equation to reduce the force of the spring closest to the acute corner is follows:

$$F_1 = W_r \frac{P_u}{2} + (W_t - W_r)P_u \qquad (2-34)$$

Where P_u is the unreduced maximum passive resistance force in each soil category.

2.3.4.2 Transverse response

The exterior shear keys, transverse resisting components in a bridge, have a significant effect on the bridge response in a seismic event. The shear keys should be designed as sacrificial elements to limit the magnitude of the transverse force which can be transmitted into the abutment.

An extensive amount of experimental research was conducted at UCSD in 2001 on the behavior of different types of shear keys. A total of 5 specimens (10 shear keys) were built at a 40% scale of the exterior shear keys of a prototype abutment. Two types of failure modes were identified for exterior shear key joints, including (1) a single horizontal crack that develops at the interface (Sliding Shear Mechanism), (2) multiple diagonal cracks along the direction of predominant principal compressive stresses (Diagonal Tension Mechanism) (Figure 2-18).The results of the experiment were dependent on the construction joint types between the abutment stem wall and

the shear key, different amount and configuration of the vertical reinforcement crossing the abutment stem wall-shear key interface and different amount and configuration of the horizontal reinforcement in the stem wall.

2.3.4.2.1 Shear Key with Sliding Shear Mechanism

Based on the experimental research of Megally et al. (2001) and Bozorgzadeh et al. (2004), Bozorgzadeh et al. (2006) proposed an equation to calculate the nominal capacity of a shear key with sliding shear failure. The deformed shape of the reinforcement of a failed shear key was taken into account to develop the equation (Figure 2-19).

$$V_n = \frac{\mu_f \cos\alpha + \sin\alpha}{1 - \mu_f \tan\beta} A_{vf} f_{su} \leq 0.2 f'_c A_C \qquad (2-35)$$

Where:
α : Angle of kinking of the vertical bars with respect to the vertical axis
β: Angle of the inclined face of shear key with respect to the vertical axis
μ_f : Kinematic coefficient of friction of concrete
A_{vf} : Amount of vertical reinforcement
f_{su} : Ultimate tensile strength of vertical reinforcement
A_C : Area of shear plane

The average kink angle α is indicated to be 37° based on experimental tests when a shear key fails. The kinematic coefficient of friction of concrete with smooth finishing is determined to be 0.36. The upper limit of nominal capacity of a shear key is the smaller of the vertical dead-load reaction at the abutment (W_a) and the summation of the total shear capacity of wing-walls and 0.75 percent of that of piles.

$$V_n \leq \min\left(W_a, 0.75V_{piles} + V_{wing-walls}\right) \qquad (2-36)$$

A trilinear backbone curve is used to model the response of the shear keys, a softening part with the stiffness equal to 2.5% of initial stiffness followed by two hardening part. The stiffness of the hardening part is assumed to be in between 0.5%-2.5% recommended by Aviram et al., 2008. A hysteretic zero length element is connected in series to another zero length element with no tension material to generate the trilinear backbone curve.

2.3.4.2.2 Shear Key with Diagonal Tension Mechanism

As can be seen in the Figure 2-20, both the vertical and horizontal reinforcement in the abutment stem wall are resisting transverse forces. The crack is developed from the shear key-abutment wall interface nearest the application point of the transverse load to reach the base of the abutment wall. Based on the equilibrium of forces in the shear key along the diagonal crack, the following equations are developed to calculate the nominal capacity of the shear key.

$$V_N = V_c + V_s \qquad (2-37)$$

$$V_C = \begin{cases} 2.4\sqrt{f'}bh & (psi) \\ 0.2\sqrt{f'}bh & (MPa) \end{cases} \qquad (2-38)$$

Where:
V_c: Concrete contribution to the shear key capacity
V_s: Steel contribution to the shear key capacity
b : The stemwall width
h : The height of abutment stemwall
f': The compressive strength of concrete

$$V_s = \left[F_P h_P + T_1 h + T_2 d + n_h T_{i,h} \frac{h^2}{2s} + n_v T_{i,v} \frac{d^2}{2s}\right]\left(\frac{1}{h+a}\right) \qquad (2-39)$$

$$T_1 = A_{s,1} f_{y,1} \qquad (2-40)$$

$$T_2 = A_{s,2} f_{y,2} \qquad (2-41)$$

$$T_{i,h} = A_{s,h} f_{y,h} \qquad (2-42)$$

$$T_{i,v} = A_{s,v} f_{y,v} \qquad (2-43)$$

Where:

T_1: The force that can be developed by the tension tie

T_2: The force that can be developed in the first row of steel bars crossing the shear key interface

$T_{i,v}, T_{i,h}$: The tensile force on a single vertical and horizontal bar placed on the side faces of the abutment stem wall crossing the inclined crack

F_P: The force caused from the stem wall being post-tensioned

$A_{s,1}$: The total area of steel along the horizontal tension tie T_1

$A_{s,2}$: The total area of steel along T_2

$A_{s,s}$: The cross sectional area of the side reinforcement

n_v, n_h : The number of side faces with horizontal and vertical side reinforcement

In general $A_{s,1} = A_{s,2} = A_{s,s}$ and $f_{y,h} = f_{y,v} = f_{y,s}$. Figure 2-21 shows the shear keys backbone curves used on this study for each specimen bridge based on the previous equations.

2.4 Tables and Figures

Table 2-1: Bridge B - Structural and Geometric Description (Kaviani et al. 2012)

Parameters	Value/Description
General Bridge description	Ordinary standard multi-column bent bridge with 2 spans
Total length of bridge	299.8 ft (91.4 m)
Abutment skew angle	0°
Number of spans and length of each deck span	2 spans: 154.82 ft (47.2 m) and 144.98 ft (44.2 m)
Total deck width (Backwall length)	75.5ft (23 m)
Deck depth (Backwall height)	6.23ft (1.9 m)
Number and clear height of each column bent	2 columns: 22ft (6.7 m)
Column diameter	5.58ft (1.7 m)
Concrete material properties for concrete of superstructure (f'_c,E_c)	Elastic deck: f'_c = 5 ksi (34.5 MPa); E_c=4030.5 ksi (27800 Mpa)
Concrete and reinforcing material properties of column bents	Concrete: f'_c = 5 ksi (34.5 MPa); Steel: ASTM A706

Table 2- 2: Bridge C - Structural and geometric description (Kaviani et al. 2012)

Parameters	Value/Description
General bridge description	Ordinary standard three columns per bent bridge with 3 spans
Total length of bridge	418.2 ft (127.5 m)
Abutment skew angle	36°
Number of spans and length of each deck span	3 spans: 156.12ft(47.6 m) + 144ft (43.9 m) + 118.08 ft (36.0 m)
Total deck width (Backwall length)	77ft (23.47 m)
Deck depth (Backwall height)	6.3ft (1.92 m)
Number and clear height of each column bent	3 columns: 24.6 ft (7.5 m)
Column diameter	5.51ft (1.68 m)
Concrete material properties for concrete of superstructure (f'_c,E_c)	Elastic deck: f'_c = 5 ksi (34.5 MPa); E_c=4030.5 ksi (27800 Mpa)
Concrete and reinforcing material properties of column bents	Concrete: f'_c = 5 ksi (34.5 MPa); Steel: ASTM A706

Table 2-3: Backfill soil type categories in California highway bridges (Earth Mechanics INC., 2005)

Category	Number of Bridges	ρ_d	w	γ	ϕ	c	ε_{50}	R_f
		(kN/m^3)	(%)	(kN/m^3)	(degree)	(kPa)		
I	2	18.9	3-6	19.4	38	0	0.0035	0.96
II	9	16.5-18.9	5-14	17.3	33	24	0.0035	0.96
III	4	17.8-17.9	7-15	19	23	96	0.0035	0.96
IV	5	14.1-18.2	14-29	14.3	6	168	0.007	0.96

Table 2-4: The ratio of reduced-resistance width ($\mathbf{W_r}$) to the tributary width ($\mathbf{W_t}$) of uniformly distributed abutment springs in the specimen bridge model (Omrani et al., 2016)

Skew Angle		15°	30°	45°
Backfill Category	I	0.4	0.8	1
	II	0.3	0.6	0.85
	III	0.2	0.4	0.6

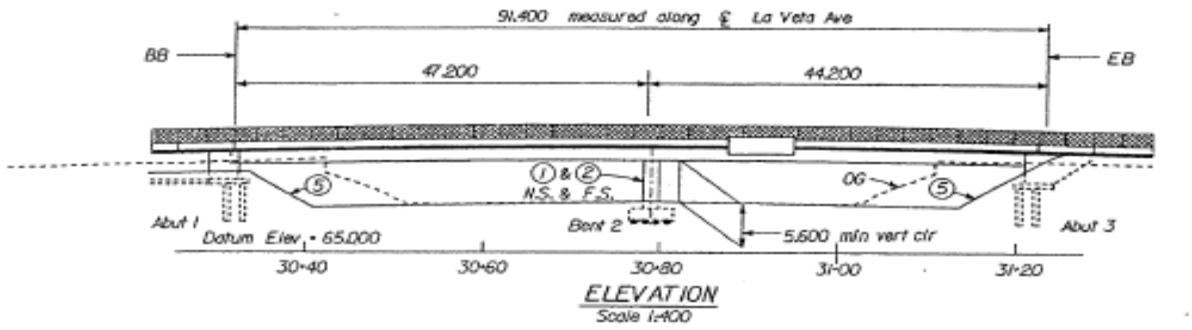

(a)

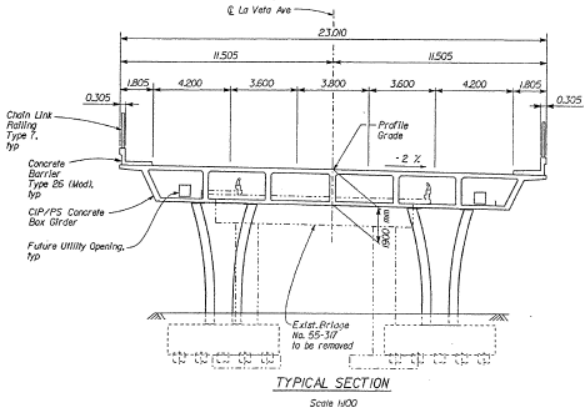

(b)

Figure 2-1(a): The La Veta Overcrossing(Bridge B) shownin elevation
(b): Typical Crosssection of the deck with columns
(Source: California Department of Transportation structural drawings)

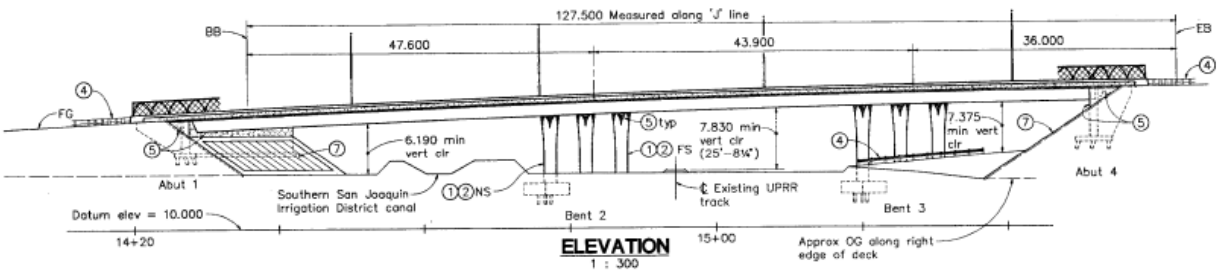

Figure 2- 2: The Jack Tone Road Overhead (Bridge C) Shown in Elevation
(Source: California Department of Transportation structural drawings)

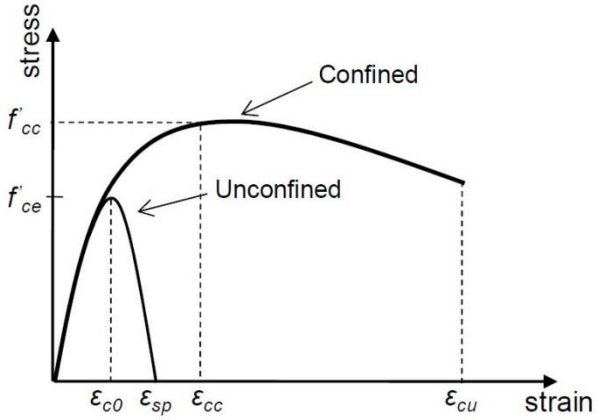

Figure 2-3: Concrete stress-strain curve (Kaviani et al. 2012)

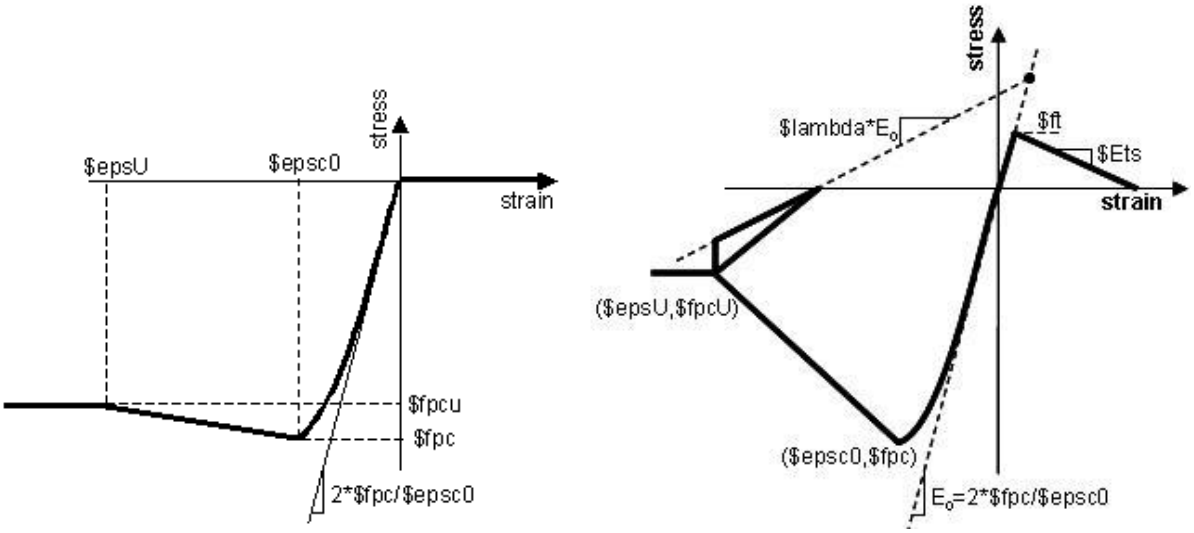

(a) (b)

Figure 2-4: Opensees concrete stress-strain curves (OpenSeesWiki)

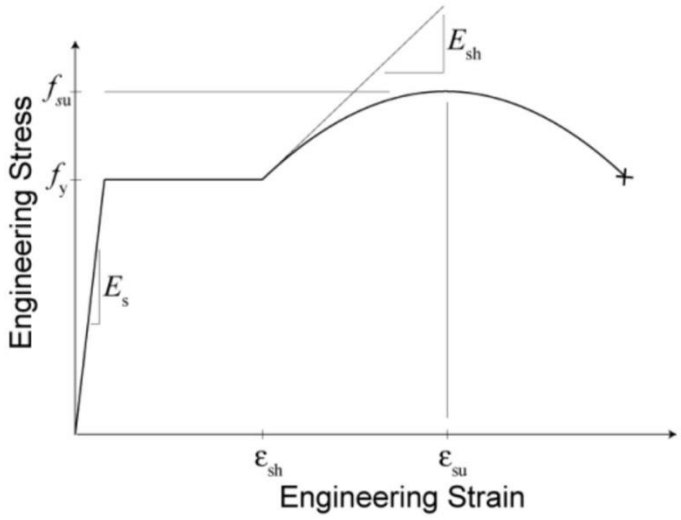

Figure 2-5: Opensees ReinforcingSteel stress-strain curve (OpenSeesWiki)

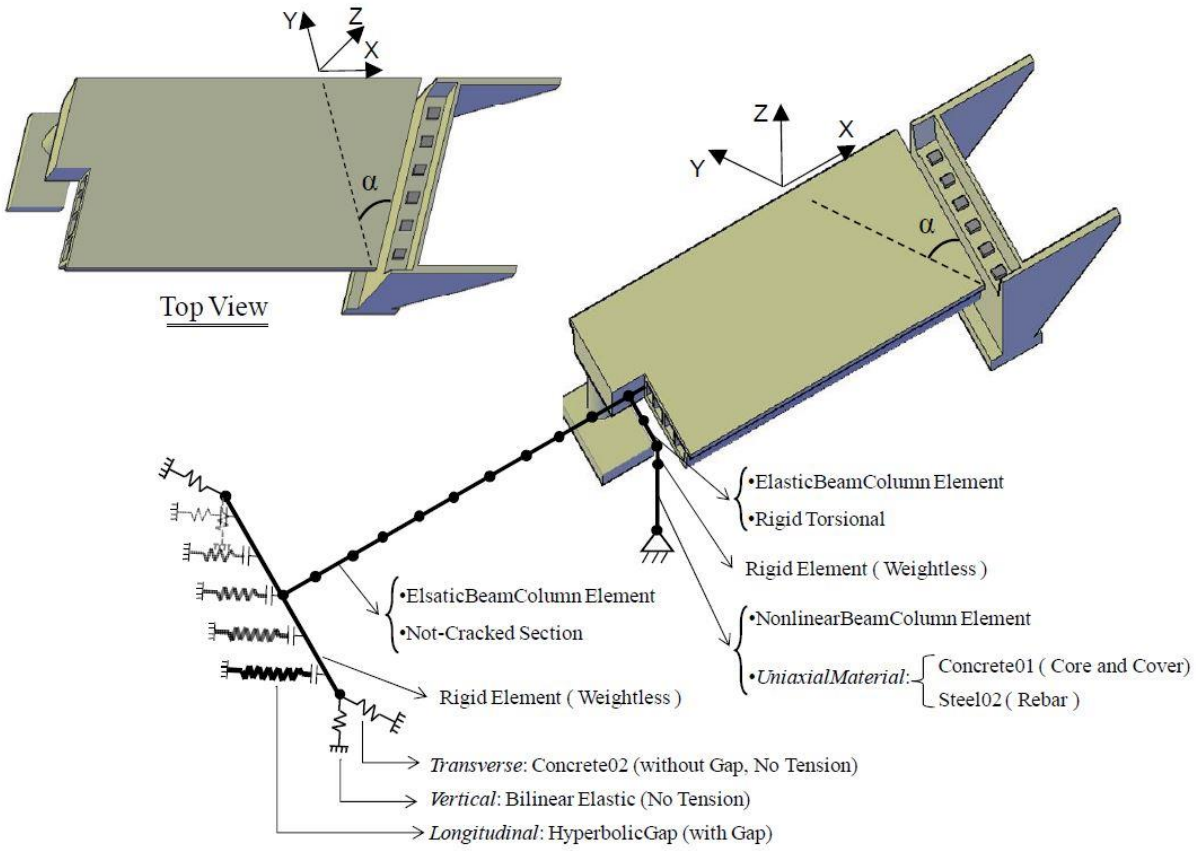

Figure 2-6: 3-D analytical bridge model (α° skew) (Kaviani et al. 2012)

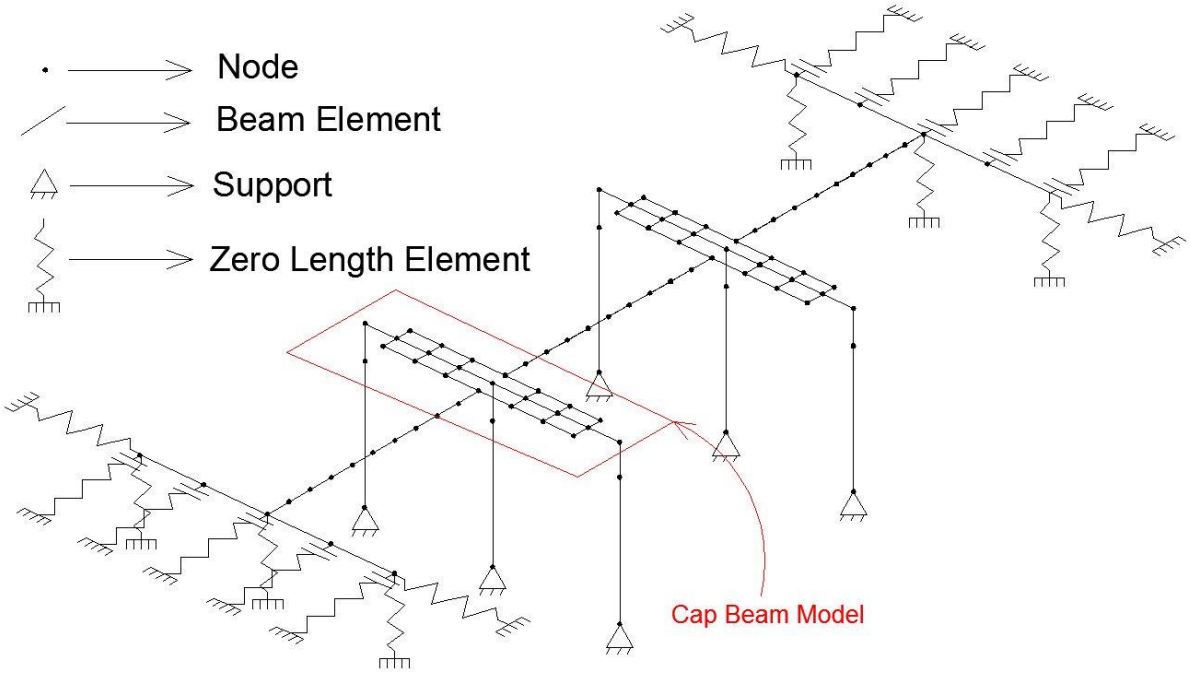

Figure 2-7: Cap beam model of Bridge C in Opensees

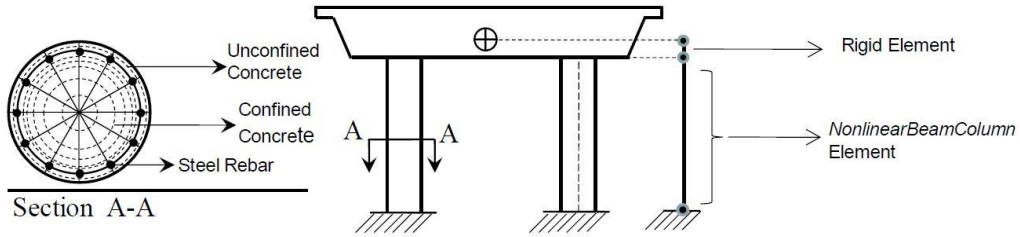

Figure 2-8: Column modeling scheme (Kaviani et al. 2012)

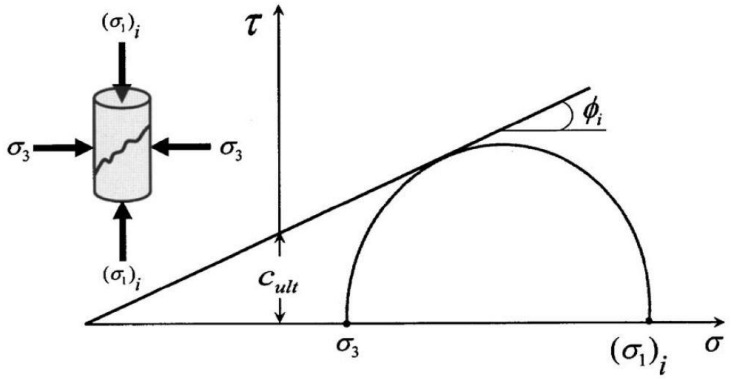

(a) Stress

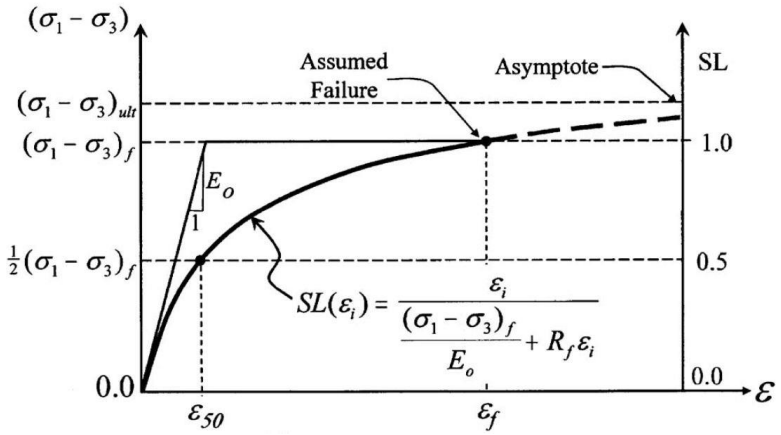

(b) Stress-Strain Relationship

Figure 2-9: Hyperbolic stress-strain relationship model (Shamsabadi et al. 2007)

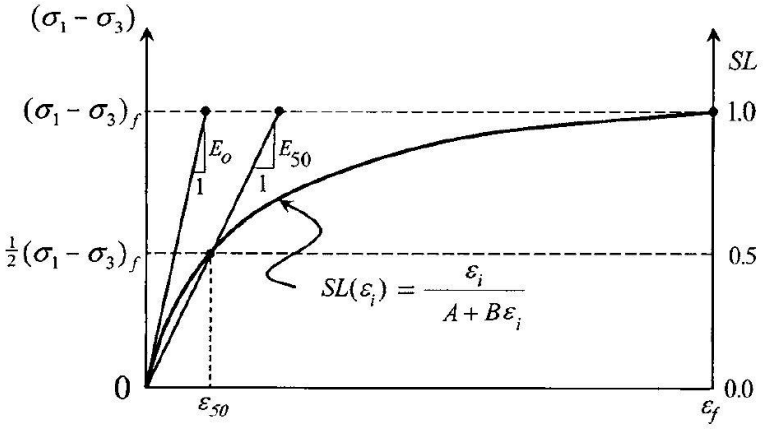

Figure 2-10: Modified hyperbolic stress-strain relationship (Shamsabadi et al. 2007)

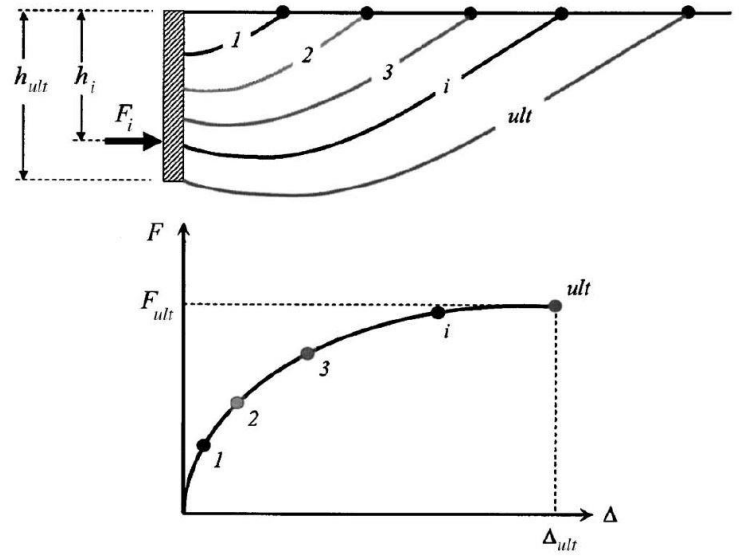

(a) Force-Displacement Relationship

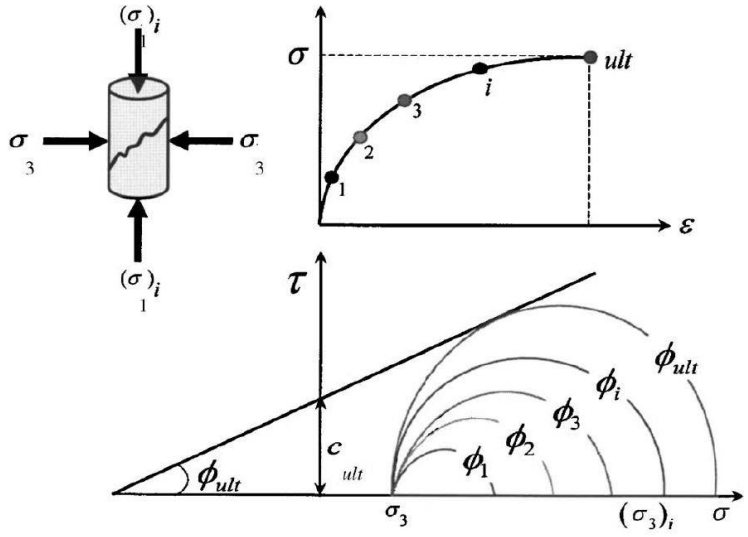

(b) Stress-Strain Relationship

Figure 2- 11: Mobilization of passive resistance (Shamsabadi et al. 2007)

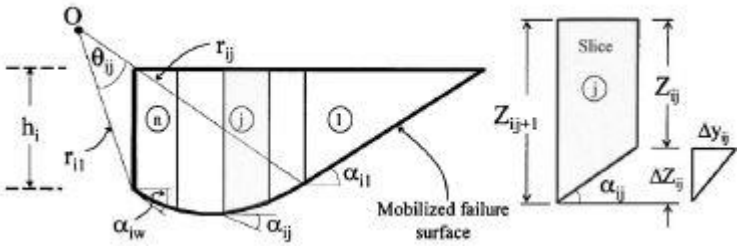

(a) Geometry

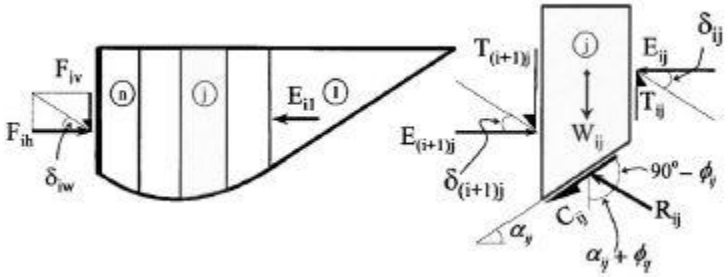

(b) Forces

Figure 2- 12: Mobilized logarithmic-spiral passive wedges (Shamsabadi et al. 2007)

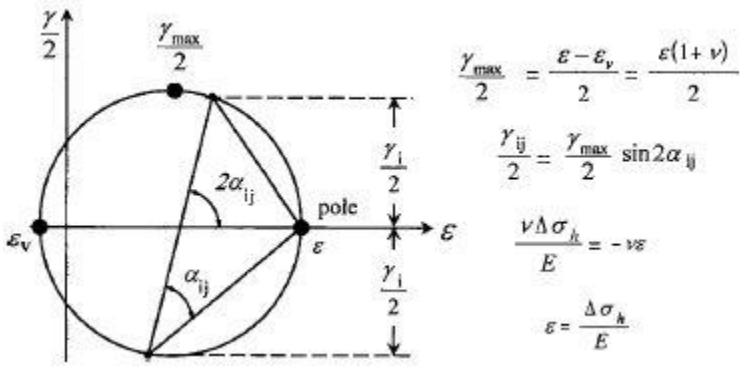

Figure 2- 13: Associated Mohr circle for soil strain in a slice (Shamsabadi et al. 2007)

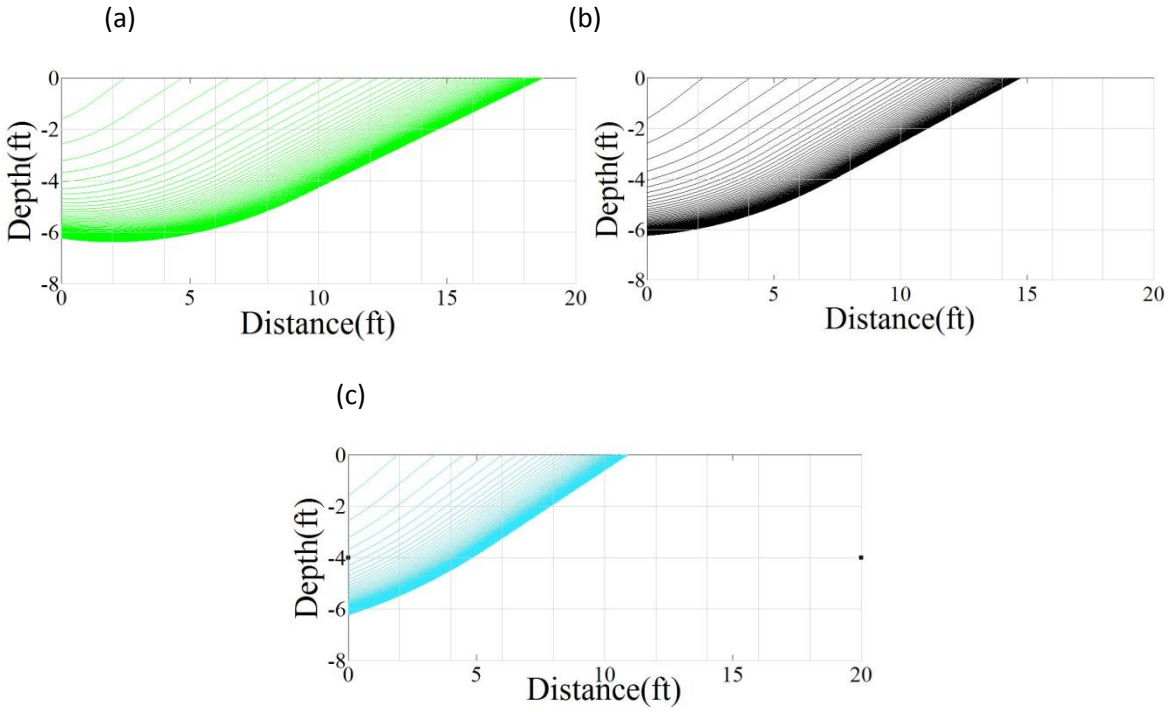

Figure 2- 14: Log-spiral hyperbolic failure surfaces (a) Category I, (b) Category II, (c) Category III

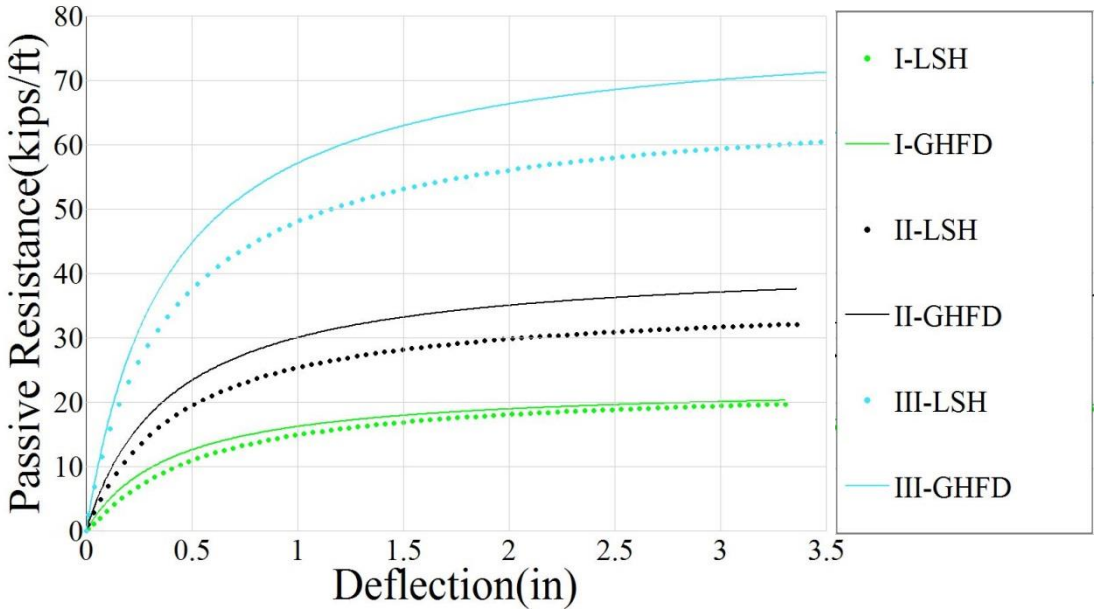

Figure 2- 15: LSH and GHFD models for the backfill soil categories I to III

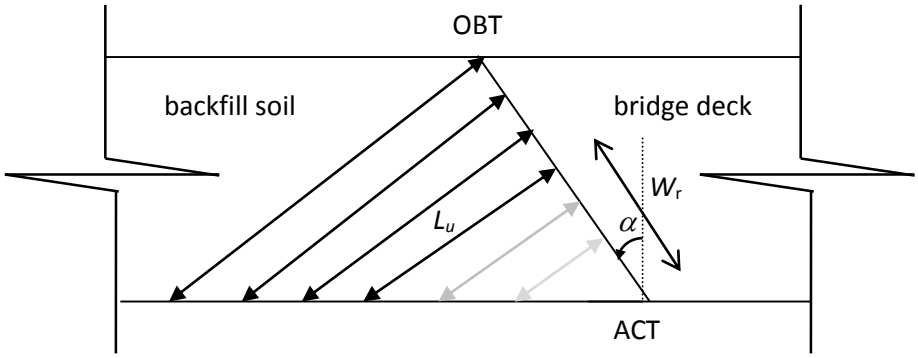

Figure 2- 16: Reduction of backfill volume normal to backfill, from the obtuse to the acute corner of a skewed abutment (Omrani et al. 2016)

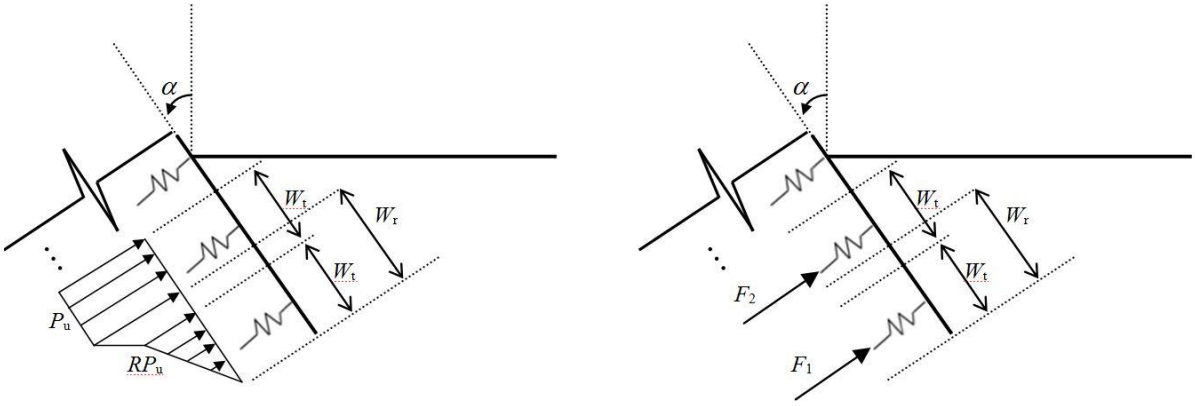

Figure 2-17: Variation of passive resistance over the reduced-resistance region in the vicinity of an acute corner in skewed abutments (Omrani et al., 2016)

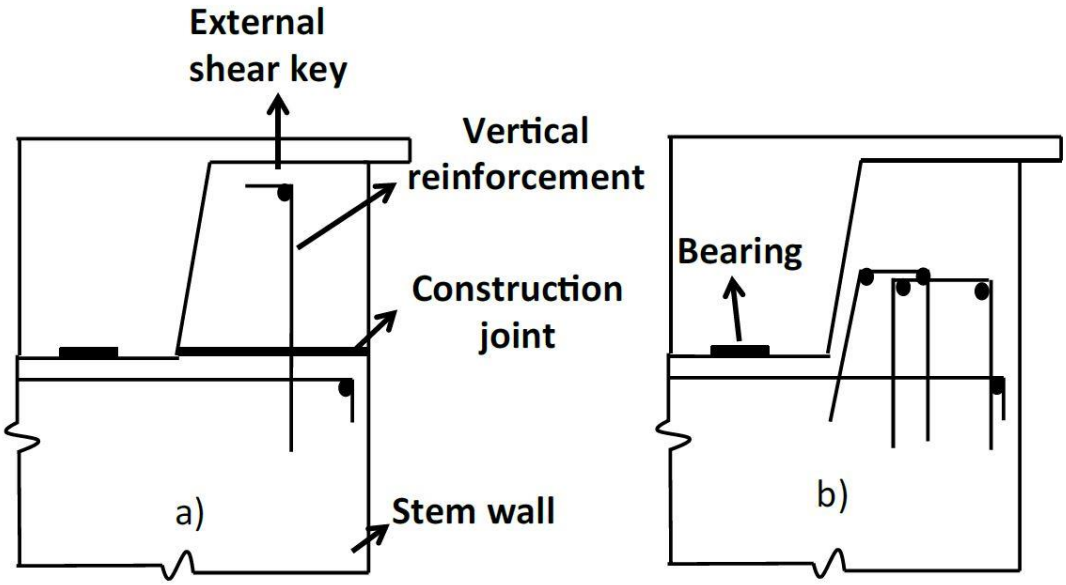

Figure 2-18: Exterior Shear Key Details: a) Shear Key with Sliding Shear Mechanism, b) Shear Key with Diagonal Tension Mechanism (SDC 2013)

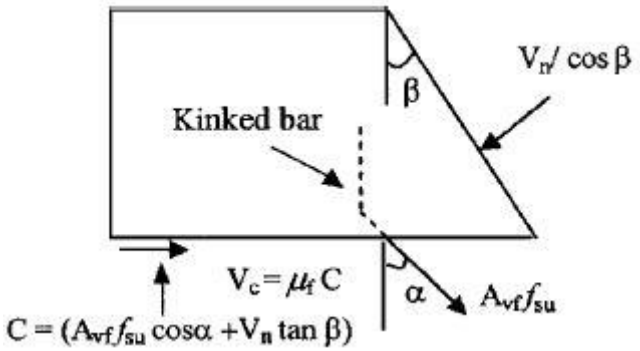

Figure 2- 19: Mechanism model of exterior shear key in shear sliding failure (Bozorgzadeh et al., 2006)

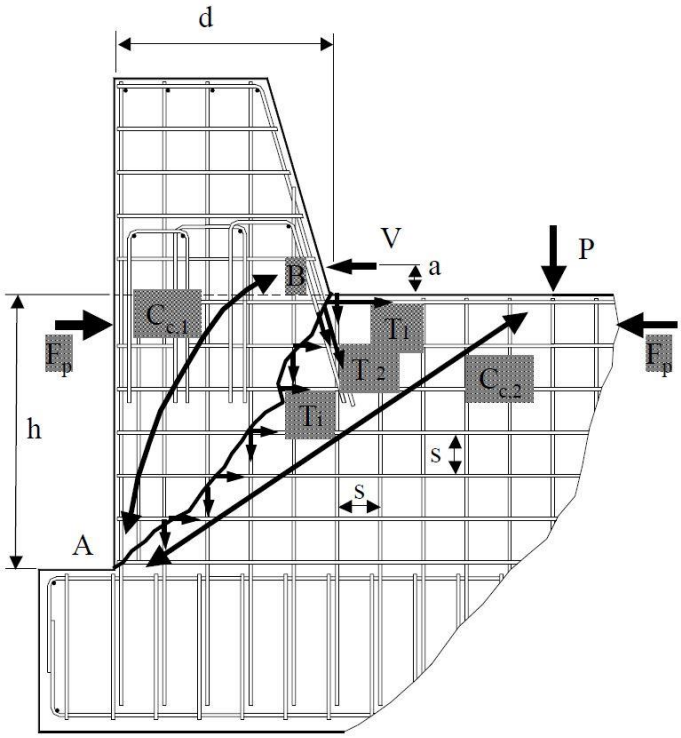

Figure 2- 20: Exterior Shear Key – Strut-and-Tie Analogous Model (Megally et al., 2001)

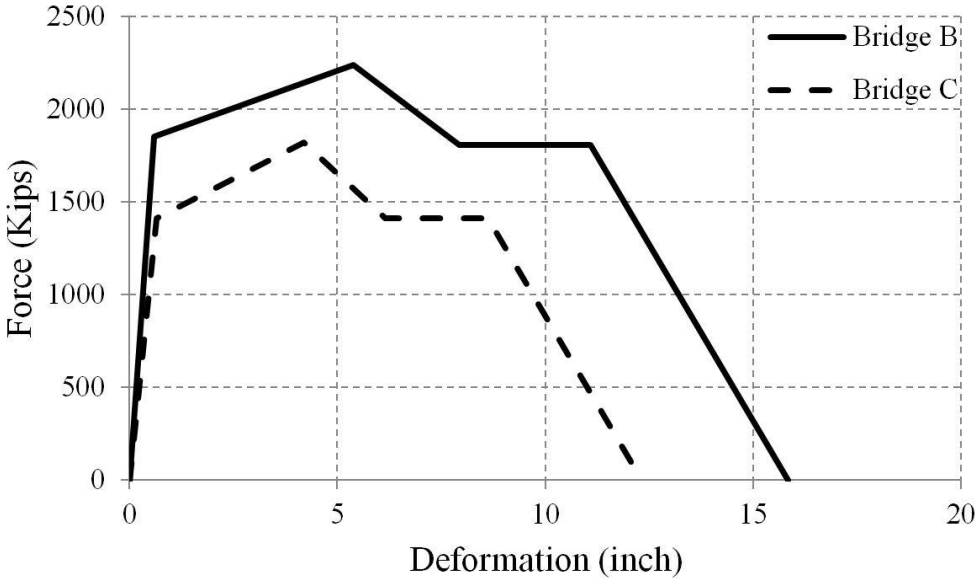

Figure 2- 21: Strut-and-tie Shear key model force-deformation backbone curve

Chapter 3

Results and Discussion

3.1 Ground Motion Selection and Application

Kaviani et al. (2012) investigated the seismic demand of various ground motions with different characteristics (Pulse-like, Soil-site, Rock-site). For high seismic demand, they used a set of 40 pulse-like ground motions which is used in this research as well. Each pair of horizontal components of the ground motions is applied at ten random incident angles to avoid any bias caused by applying them in a specific direction per Kaviani et al. (2012) recommendation. Peak Ground Velocity (PGV) is used in this study as the intensity measure which was recommended by Kaviani et. al 2012 as the most efficient intensity measure.

3.2 Collapse Criteria

The bridge collapse is determined based on the following failure criteria: 1) Column Drift Ratio (CDR) exceeding 8% that was suggested by Hutchinson et al. (2004), 2) Deck unseating which happens when the bridge deck displaces more than the abutment seat length in the longitudinal direction. Bridge B has unseating length of 86 cm and Bridge C's unseating length is 90 cm. Since the number of collapse cases is low(less than 1%), their effects are not significant in the performance assessment of the bridge specimens.

3.3 Development of Alpha Comparison Factor

Displacement Ductility Demand is a measure of the imposed post-elastic deformation on a member (SDC 2013) and is defined by the following equation:

$$\mu_D = {}^{\Delta_D}/_{\Delta_Y}$$

Where:
Δ_D: The demand displacement taken from the observed Opensees output data
Δ_Y: The yield displacement of a column from its initial position to the formation of plastic hinge calculated from pushover analysis of the bents in bridge specimens.

To be able to compare the effect of skew angle on the ductility demand of different cases regardless of the design criteria, a comparison factor denoted as α was developed.α is representative of ductility demand of a skewed bridge relative to that of the same bridge without a skewed abutment and defined as follows:

$$\alpha = \frac{\mu_{GM(i)}^{S\theta^\circ}}{\mu_{GM(i)}^{S0^\circ}}$$

Where:
$\mu_{GM(i)}^{S\theta^\circ}$: Ductility demand of a column for the case that the bridge specimen is skewed for $\theta°$ and is subjected to the ith ground motion
$\mu_{GM(i)}^{S0^\circ}$: Ductility demand of a column for the case that the bridge specimen is not skewed and is subjected to the ith ground motion

Figure 3-1 - 3-12 show the relationship between α factor and peak ground velocity (PGV) for three different abutment skew angles. As can be seen in all of the figures, the slope of the linear regression lines fit to the data is negligible. It is concluded that the relationship in between α and PGV is negligible. As a result, the regression line is defined by a constant value equal to the median of α in each case. Therefore, the effect of the abutment skew angle on the ductility demand of the bridges in different cases is investigated by exploring the 16th, 50th, and 84th

percentile α values relative to the skew angle. Part (d) of Figure 3-1 to 3-12 illustrate that median and the dispersion values of α grow when the abutment skew angle increases while keeping the value of other parameters the same in each case.

Figures 3-13 to 3-19 show that the median value of α at three representative skew angles for all cases of backfill modeling in both bridge specimens with brittle and ductile shear key, respectively. The figures show that as the backfill soil becomes more cohesive, the median values of α increase.

Figure 3-17 to 3-22 show the effect of shear key ductility on the global ductility demand of each of the skewed bridges. The α value, representative of ductility demand of a skewed bridge to the same non-skewed bridge, remains approximately the same for all skew angles and different backfill models in bridge B when the shear keys ductility is changed based on the Figures 3-17 to 3-19. In Bridge C, however, ductility demand for the bridge with brittle shear key is more than that of the bridge with ductile shear key. Furthermore, the difference of α value in Bridge C with ductile and brittle shear key at each abutment skew angle is increasing gradually as the backfill soil behind the abutment becomes more cohesive according to the Figure 3-20 to 3-22. The difference becomes noticeable for the case with the most cohesive soil for the backfill which has the most resistance force (Figure 3-22). The main reason is postulated that Bridge C has higher rotational stiffness. Therefore, Bridge C has lower rotation compared to bridge B.

For comparing the ductility demand in two specimen bridges, plots in Figures 3-23 to 3-28 are developed. As can be seen in Figures 3-23 to 3-25, except for backfill category III, Bridge B with brittle shear key shows slightly higher ductility demand compared to Bridge C with brittle shear key for all abutment skew angles. The difference in between the ductility demand in the

specimen bridges is more noticeable for all cases when ductile shear key is used. Bridge B has lower resistance to rotation compared to Bridge C because of having lower number of bents and columns. Therefore, it can be concluded from the results that Bridge B has higher ductility demand than Bridge C.

3.4 Tables and Figures

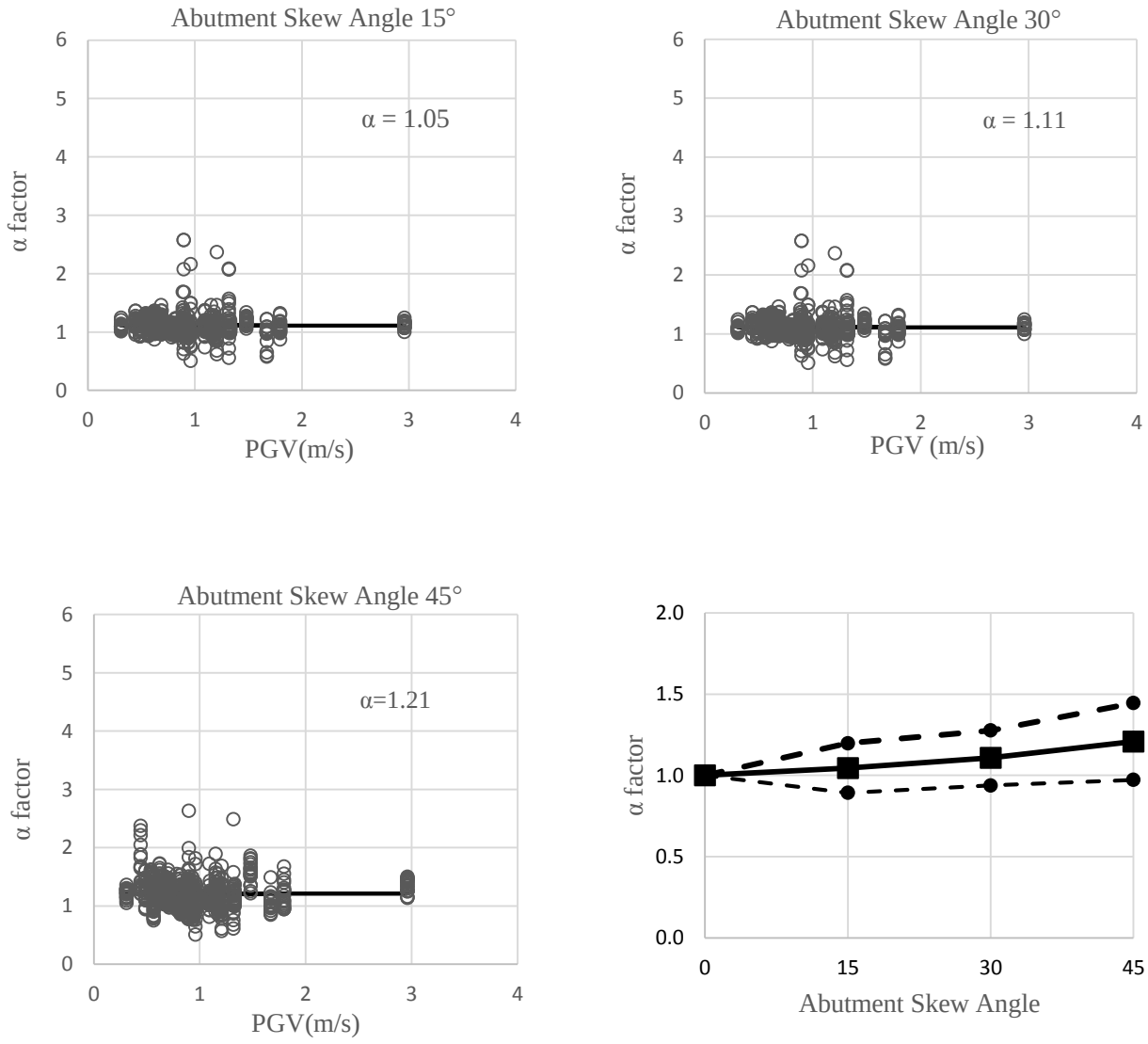

Figure 3-1: Variation of α factor with PGV in Bridge B with Category I GHFD backfill model and Brittle Shear key at a) 15°skewed abutment, b) 30°skewed abutment, c) 45°skewed abutment ,d) Variation of α factor with abutment skew angle

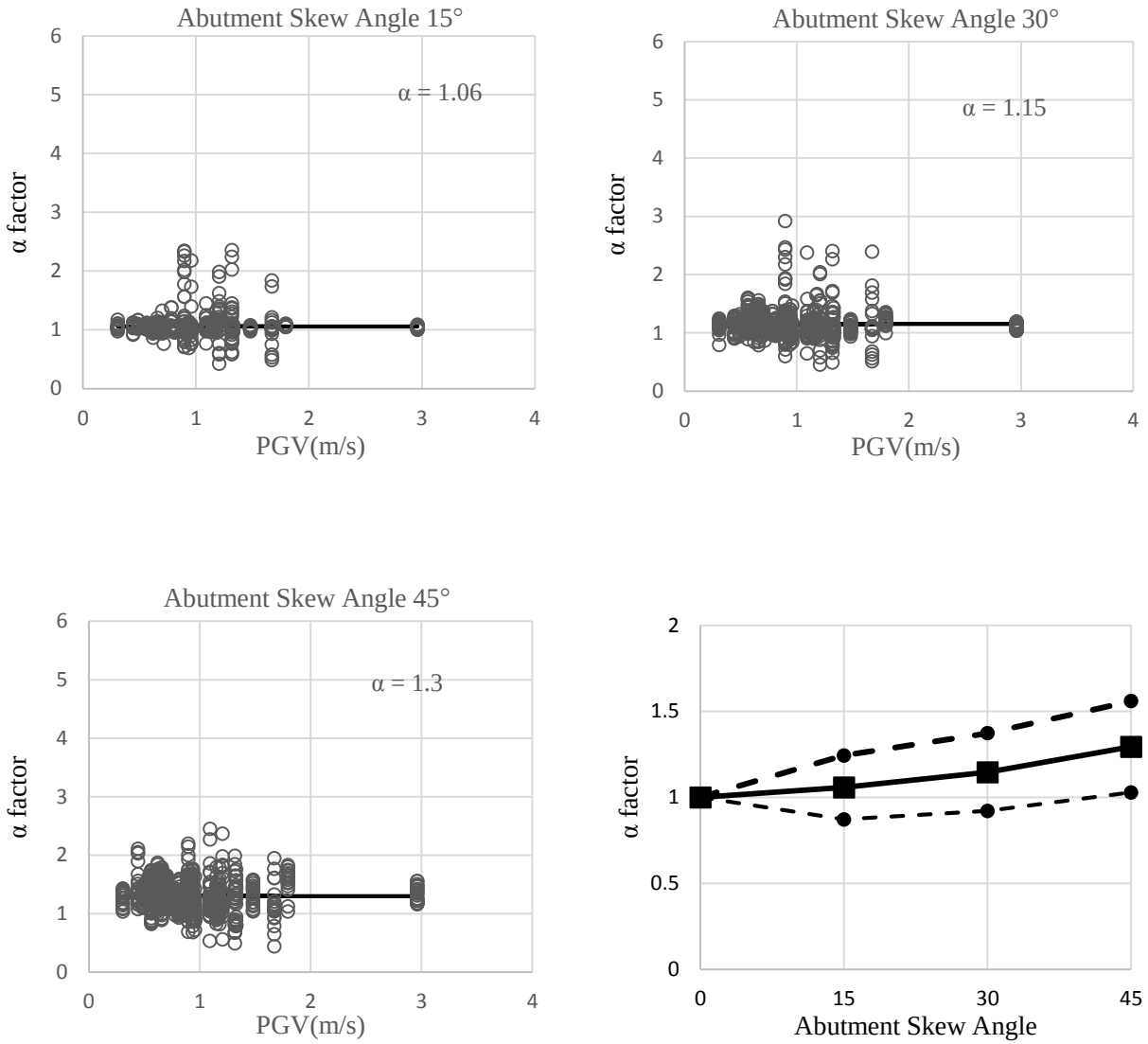

Figure 3-2: Variation of α factor with PGV in Bridge B with Category II GHFD backfill model and Brittle Shear key at a) 15°skewed abutment, b) 30°skewed abutment, c) 45°skewed abutment ,d) Variation of α factor with abutment skew angle

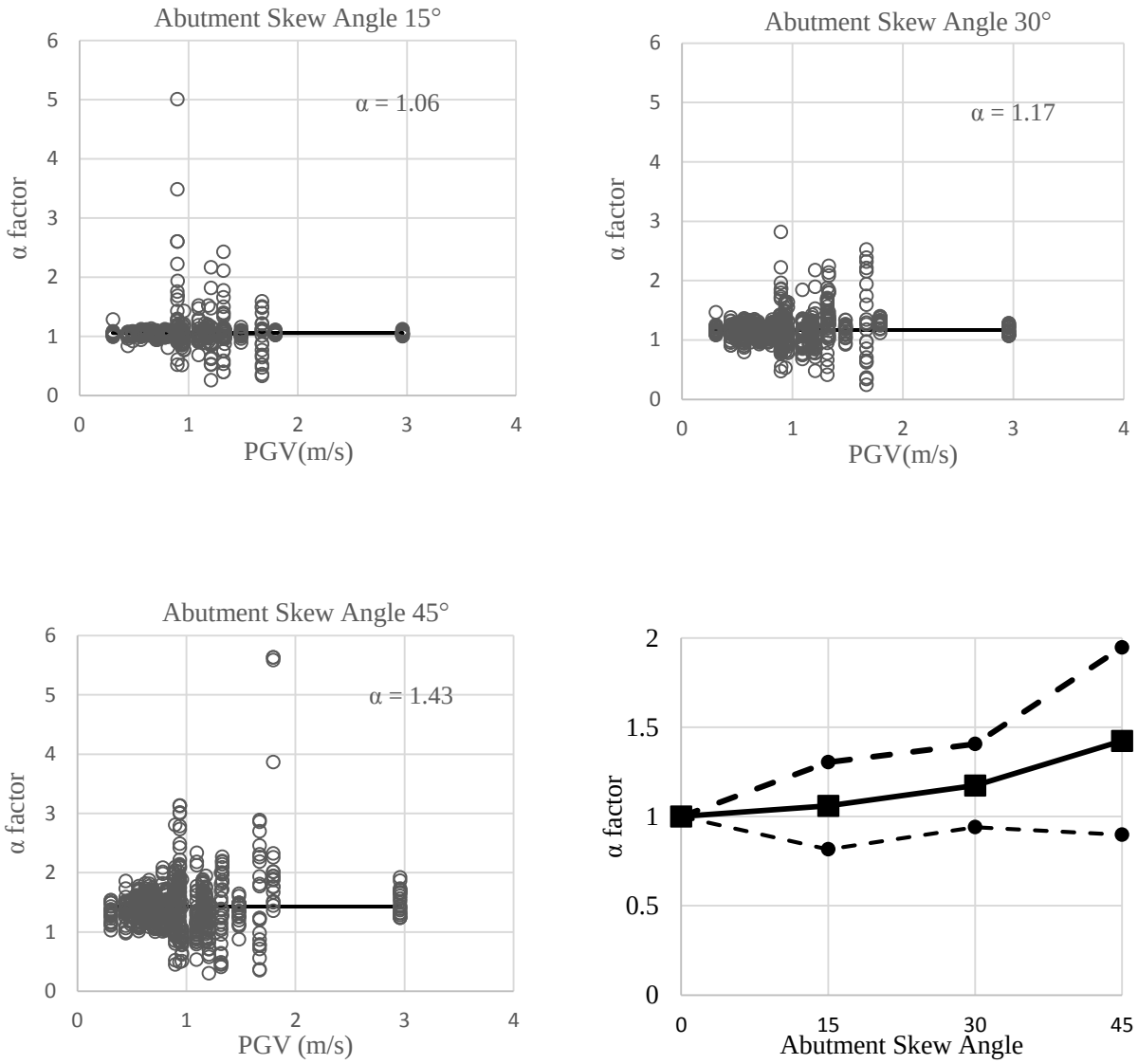

Figure 3-3: Variation of α factor with PGV in Bridge B with Category III GHFD backfill model and Brittle Shear key at a) 15°skewed abutment, b) 30°skewed abutment, c) 45°skewed abutment ,d) Variation of α factor with abutment skew angle

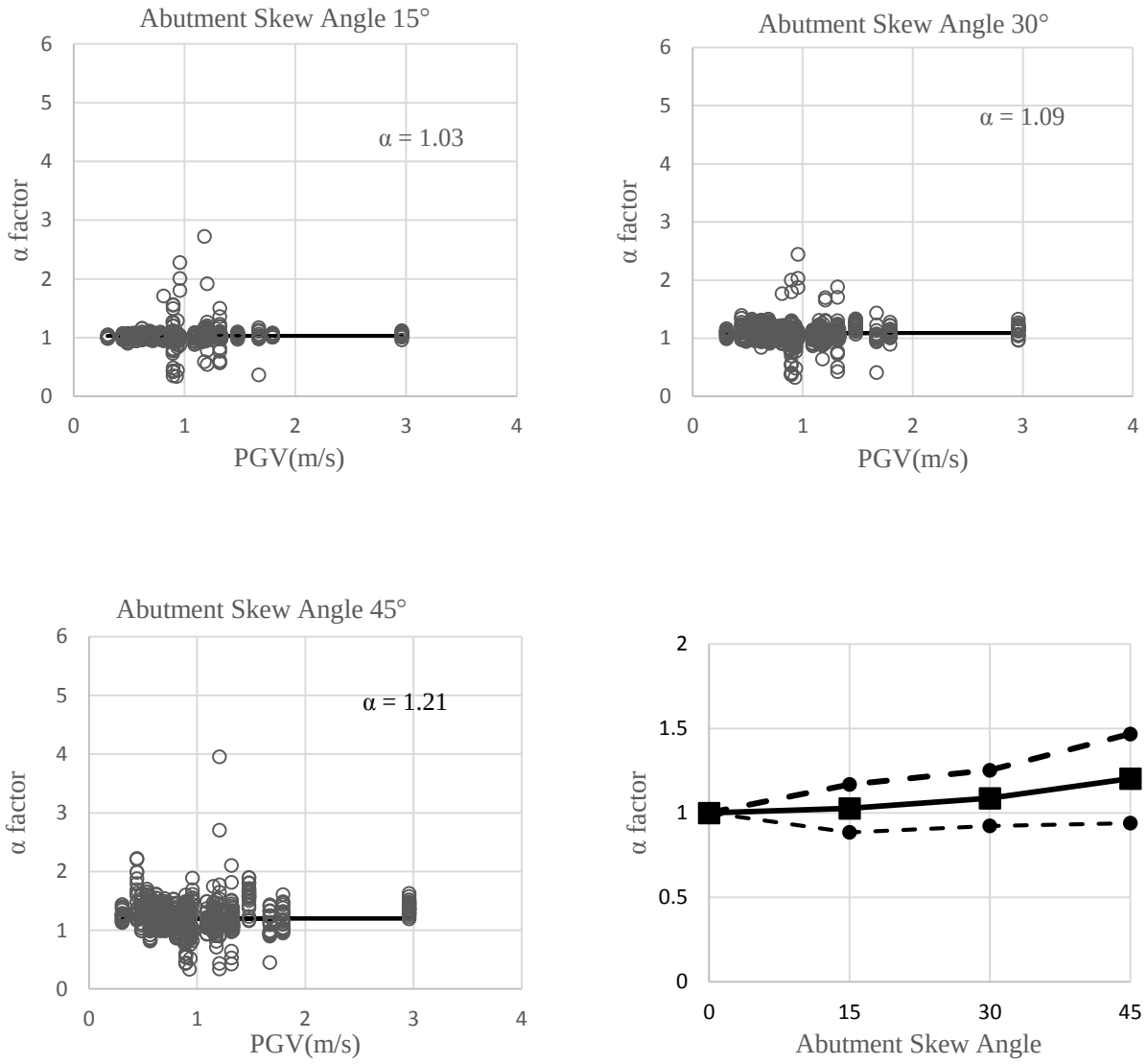

Figure 3-4: Variation of α factor with PGV in Bridge B with Category I GHFD backfill model and Ductile Shear key at a) 15°skewed abutment, b) 30°skewed abutment, c) 45°skewed abutment ,d) Variation of α factor with abutment skew angle

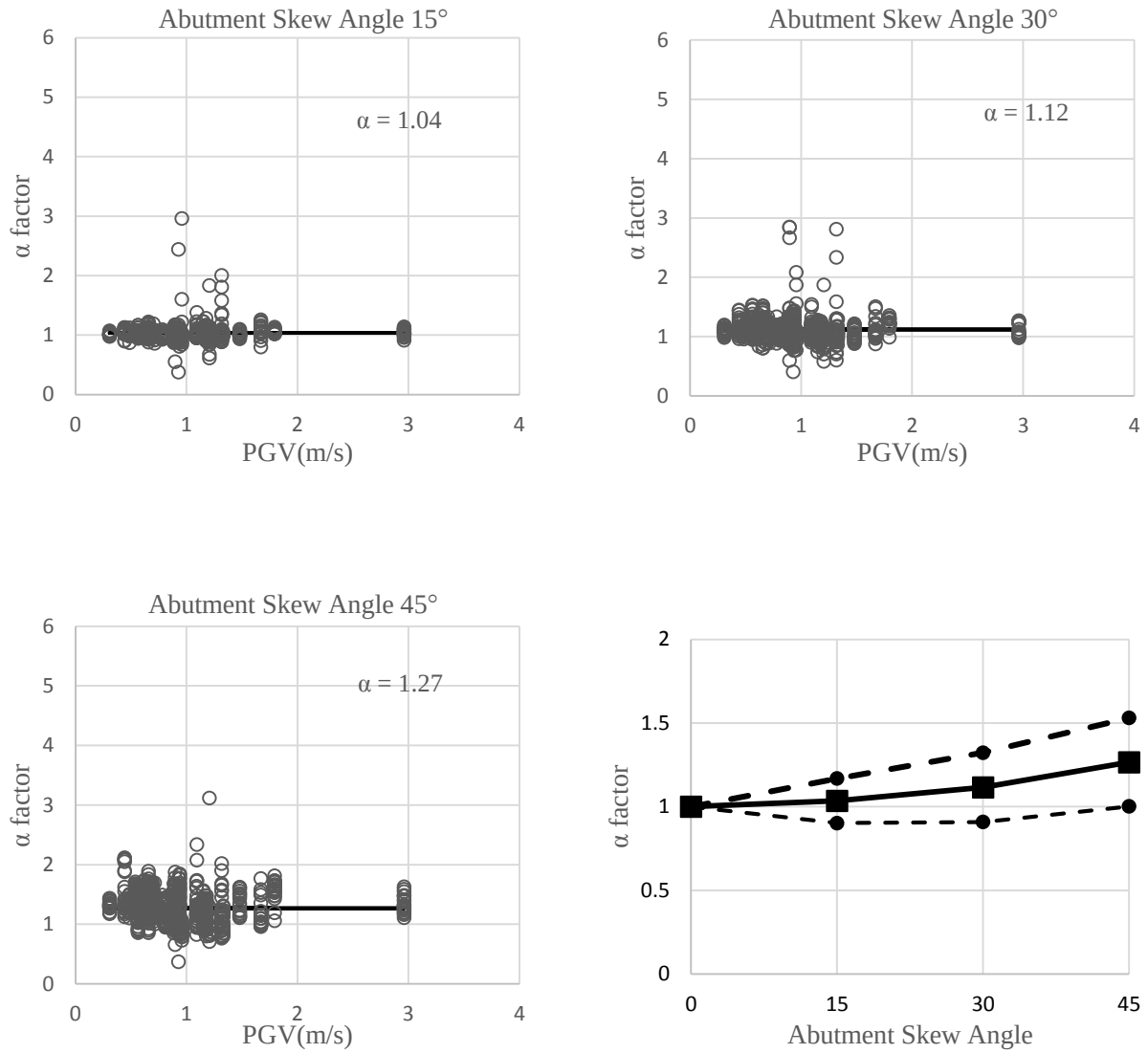

Figure 3-5: Variation of α factor with PGV in Bridge B with Category II GHFD backfill model and Ductile Shear key at a) 15°skewed abutment, b) 30°skewed abutment, c) 45°skewed abutment ,d) Variation of α factor with abutment skew angle

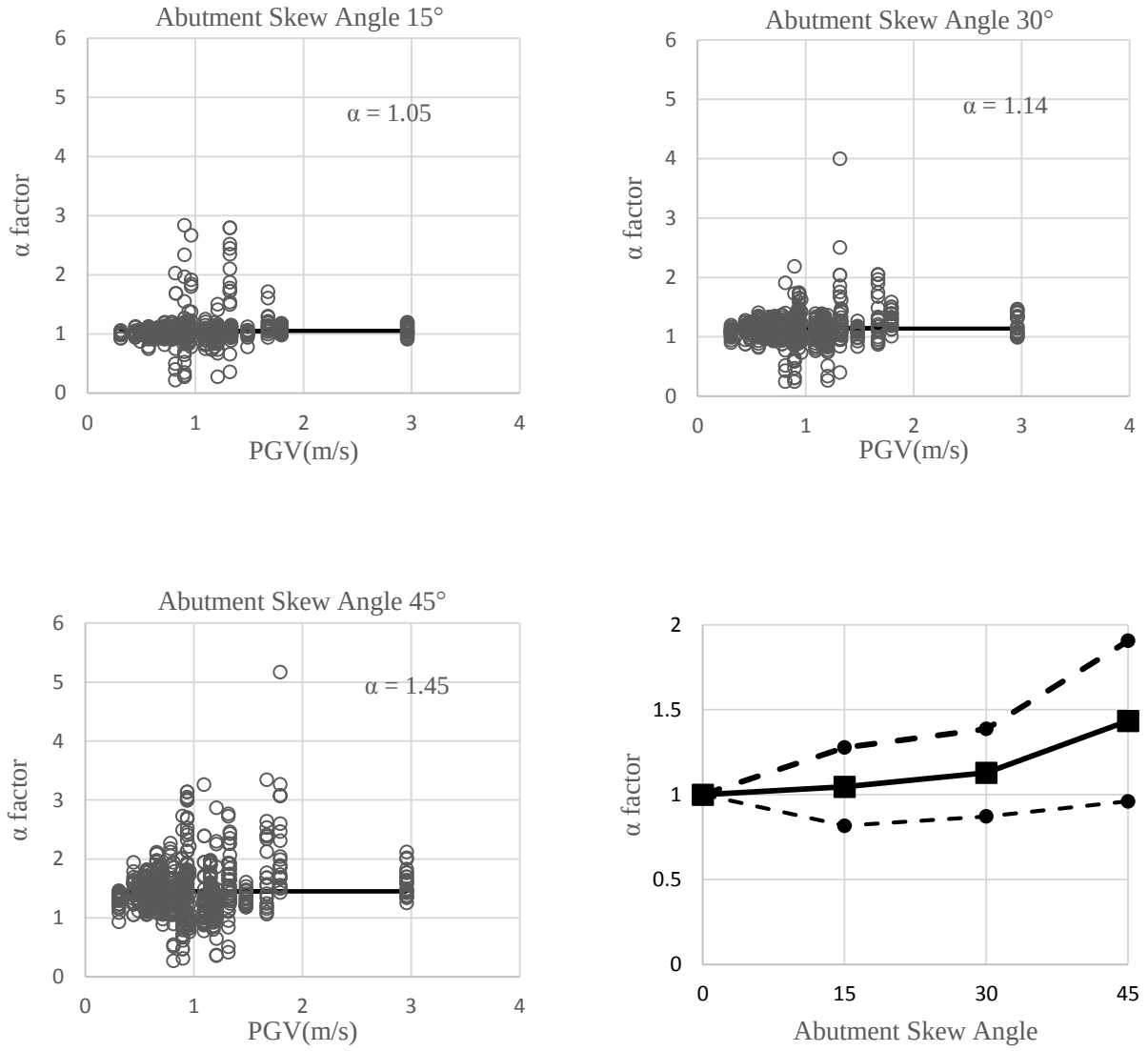

Figure 3-6: Variation of α factor with PGV in Bridge B with Category III GHFD backfill model and Ductile Shear key at a) 15°skewed abutment, b) 30°skewed abutment, c) 45°skewed abutment ,d) Variation of α factor with abutment skew angle

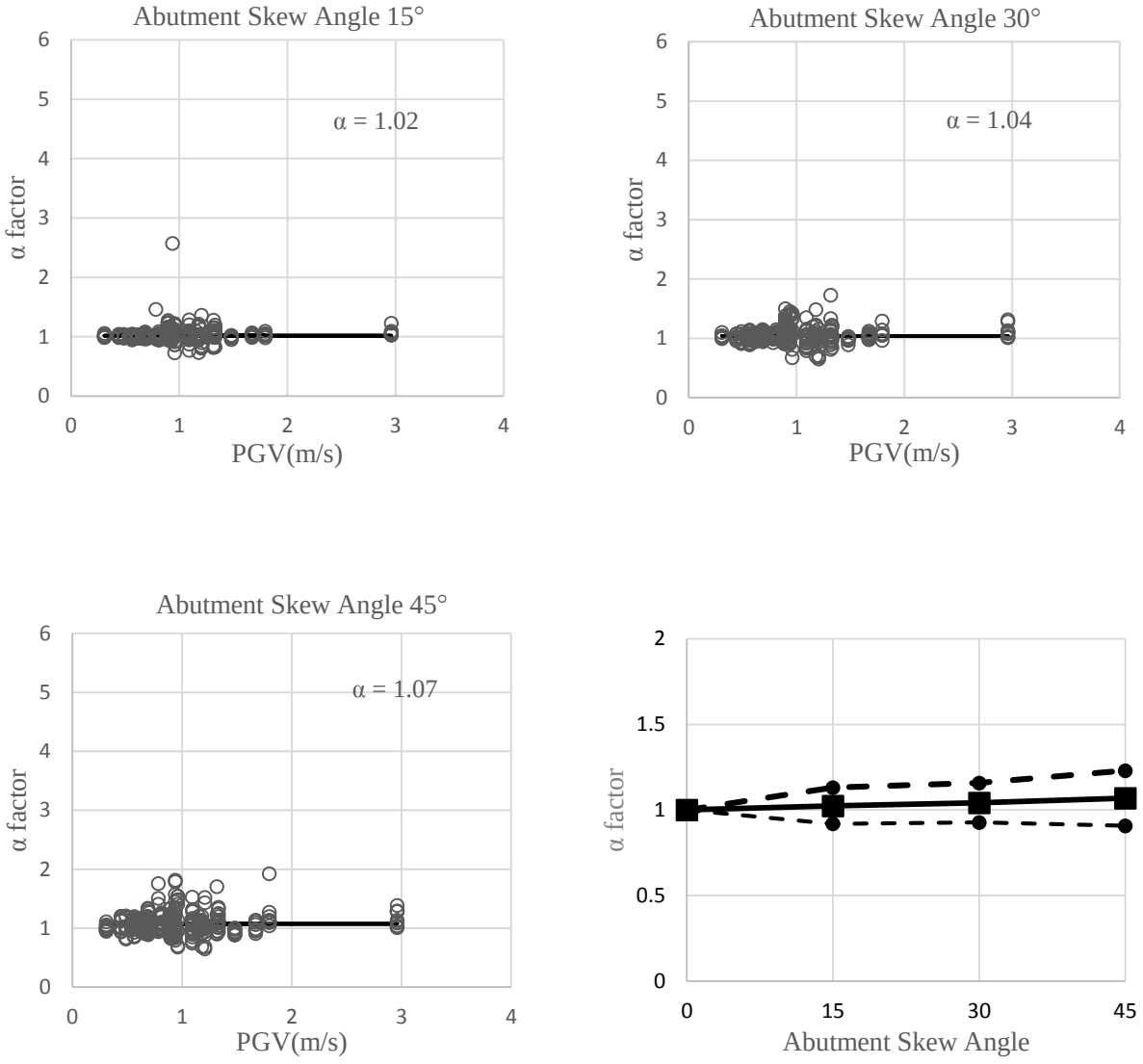

Figure 3-7 Variation of α factor with PGV in Bridge C with Category I GHFD backfill model and Brittle Shear key at a) 15°skewed abutment, b) 30°skewed abutment, c) 45°skewed abutment ,d) Variation of α factor with abutment skew angle

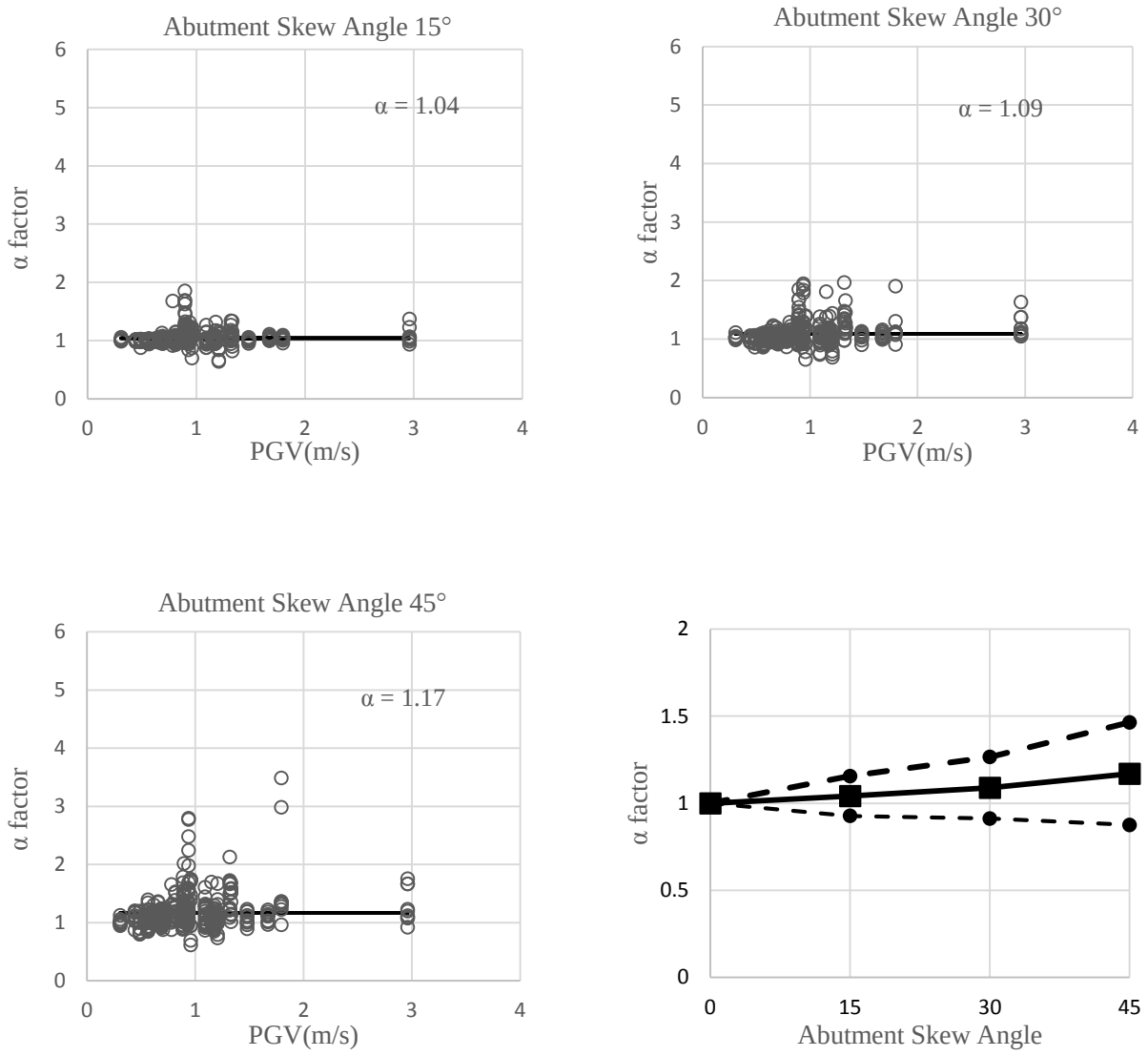

Figure 3-8: Variation of α factor with PGV in Bridge C with Category II GHFD backfill model and Brittle Shear key at a) 15°skewed abutment, b) 30°skewed abutment, c) 45°skewed abutment ,d) Variation of α factor with abutment skew angle

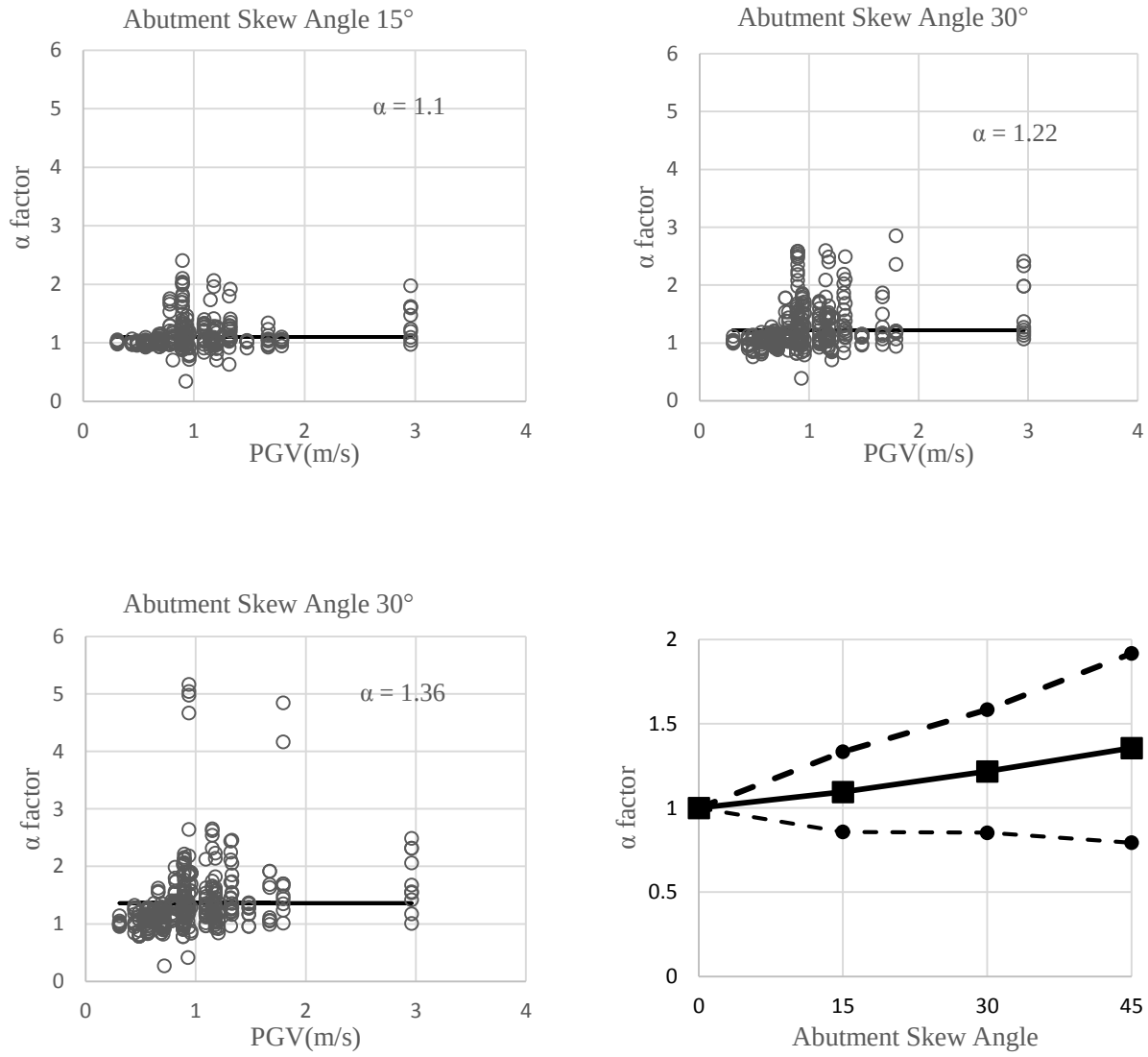

Figure 3-9: Variation of α factor with PGV in Bridge C with Category III GHFD backfill model and Brittle Shear key at a) 15°skewed abutment, b) 30°skewed abutment, c) 45°skewed abutment ,d) Variation of α factor with abutment skew angle

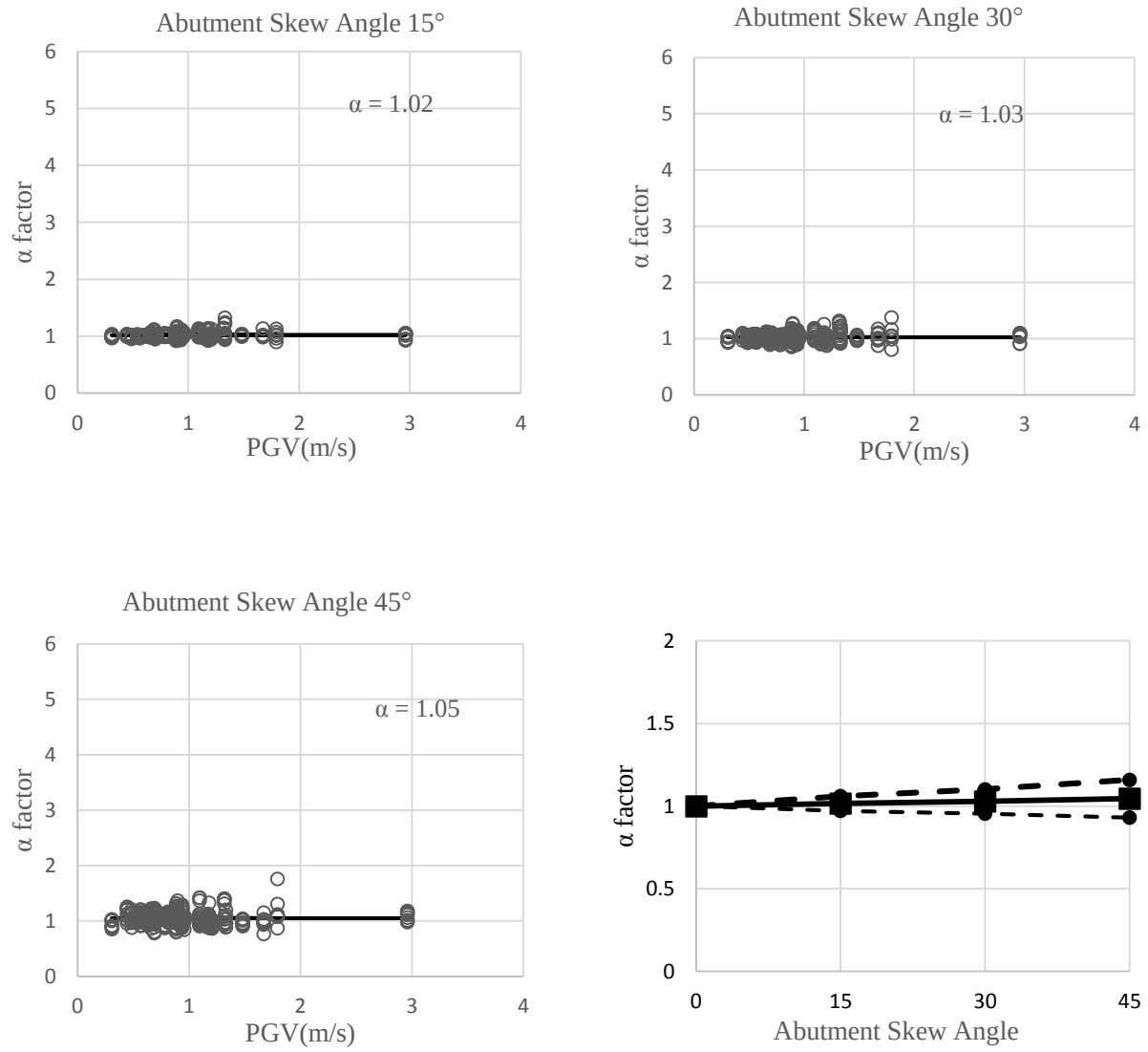

Figure 3-7: Variation of α factor with PGV in Bridge C with Category I GHFD backfill model and Ductile Shear key at a) 15°skewed abutment, b) 30°skewed abutment, c) 45°skewed abutment ,d) Variation of α factor with abutment skew angle

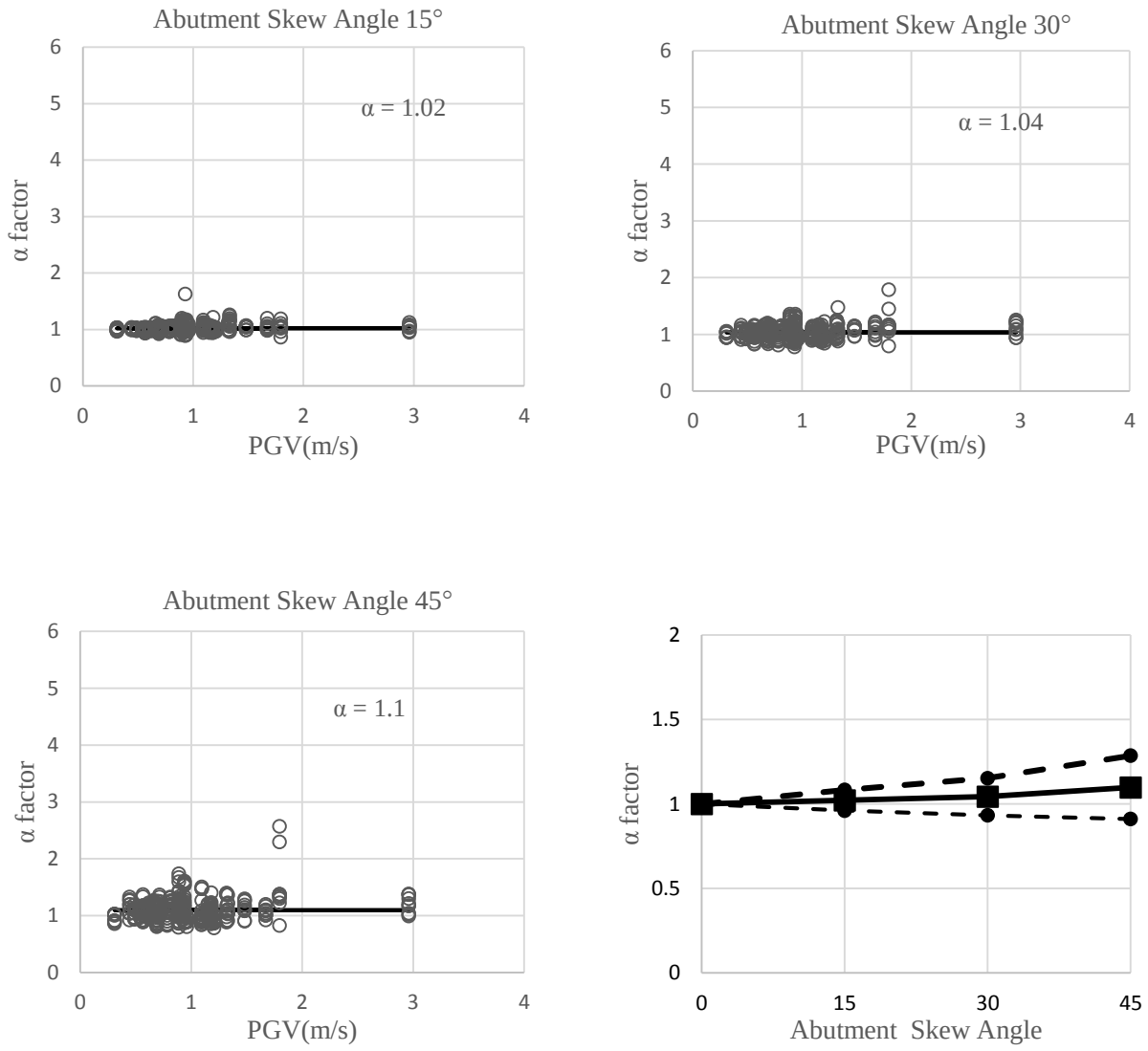

Figure 3-11: Variation of α factor with PGV in Bridge C with Category II GHFD backfill model and Ductile Shear key at a) 15°skewed abutment, b) 30°skewed abutment, c) 45°skewed abutment ,d) Variation of α factor with abutment skew angle

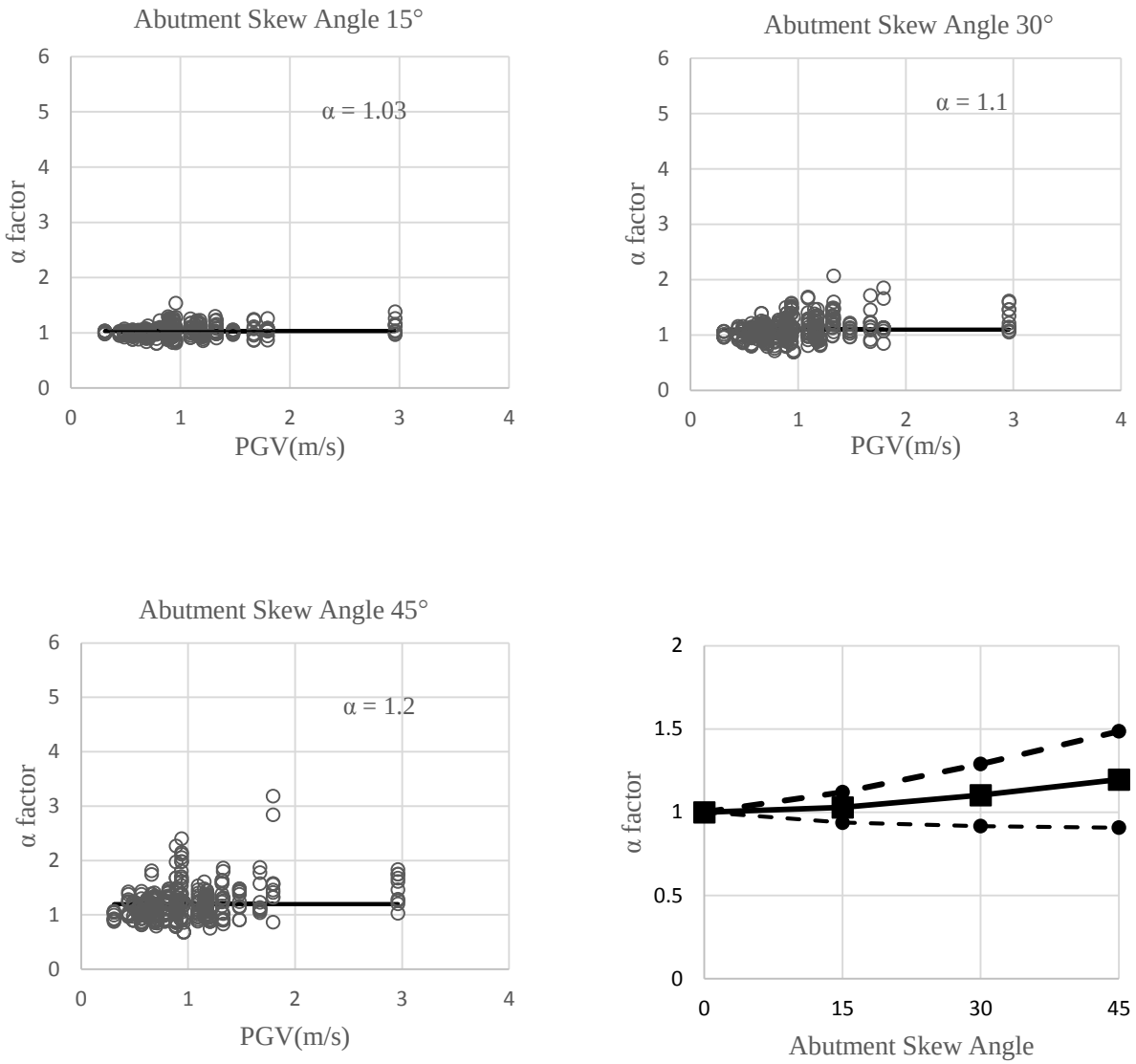

Figure 3-8: Variation of α factor with PGV in Bridge C with Category III GHFD backfill model and Ductile Shear key at a) 15°skewed abutment, b) 30°skewed abutment, c) 45°skewed abutment ,d) Variation of α factor with abutment skew angle

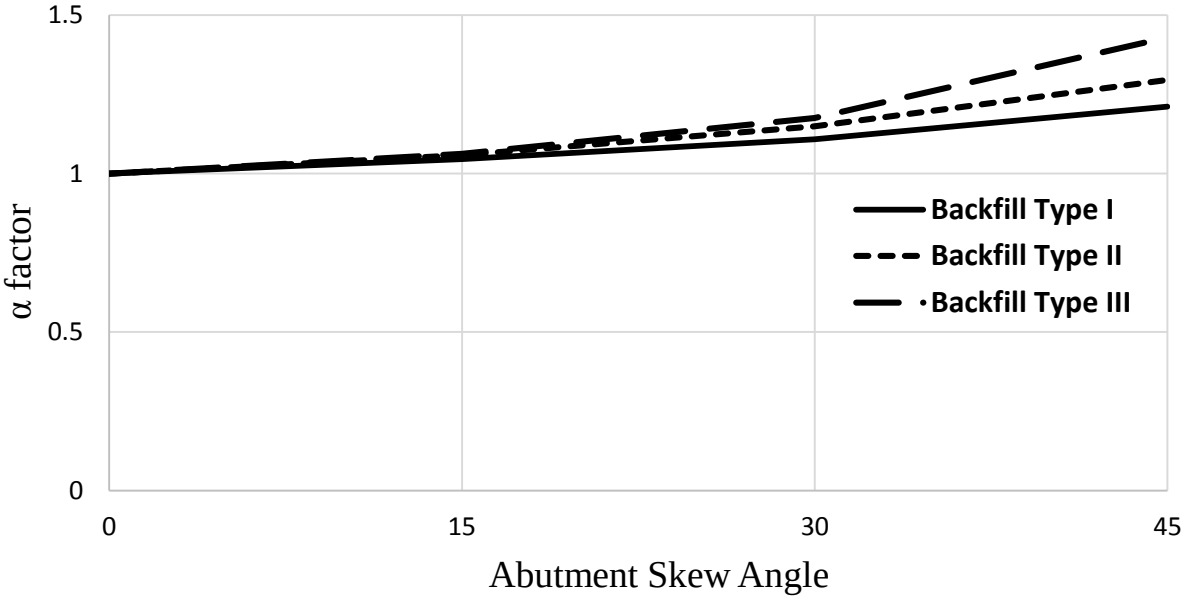

Figure 3-13: comparison of $\boldsymbol{\alpha}$ factor in Bridge B with three representative GHFD backfill models (Soil Category I to III) and brittle shear key

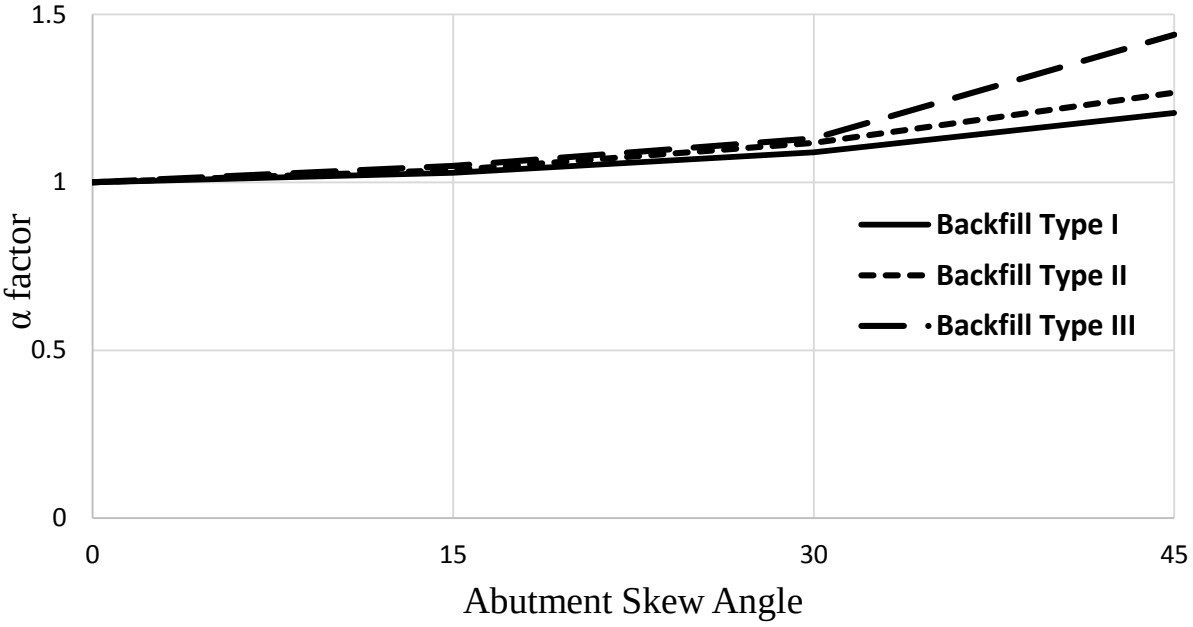

Figure 3-14: Comparison of $\boldsymbol{\alpha}$ factor in Bridge B with three representative GHFD backfill models (Soil Category I to III) and ductile shear key

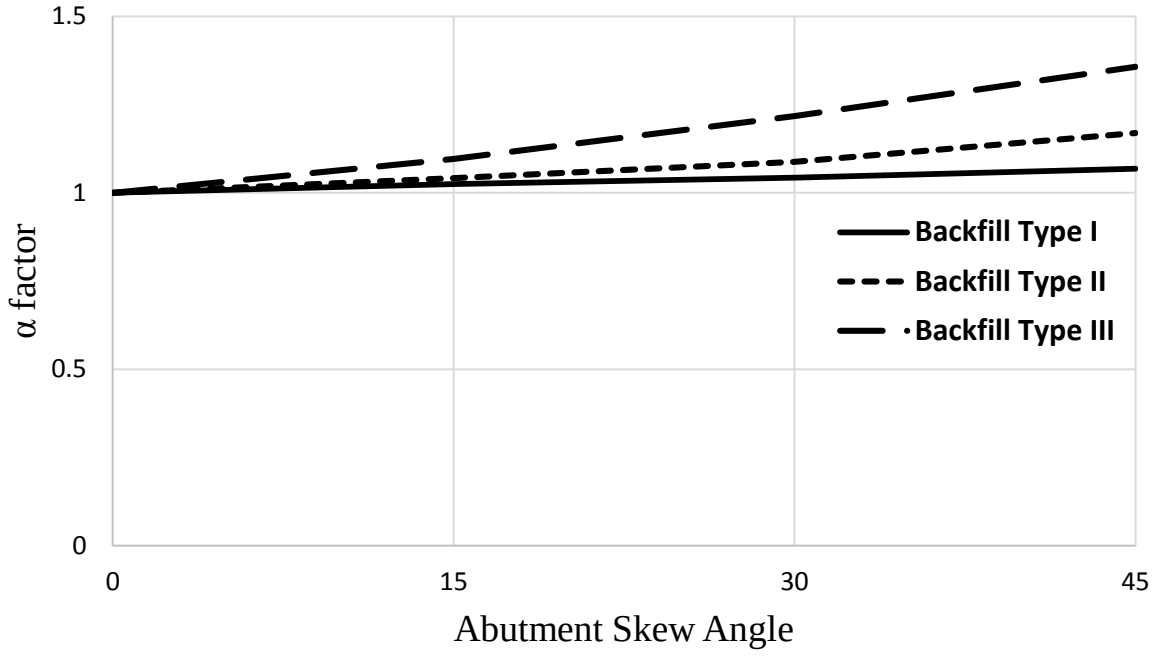

Figure 3- 15: comparison of α factor in Bridge C with three representative GHFD backfill models (Soil Category I to III) and brittle shear key

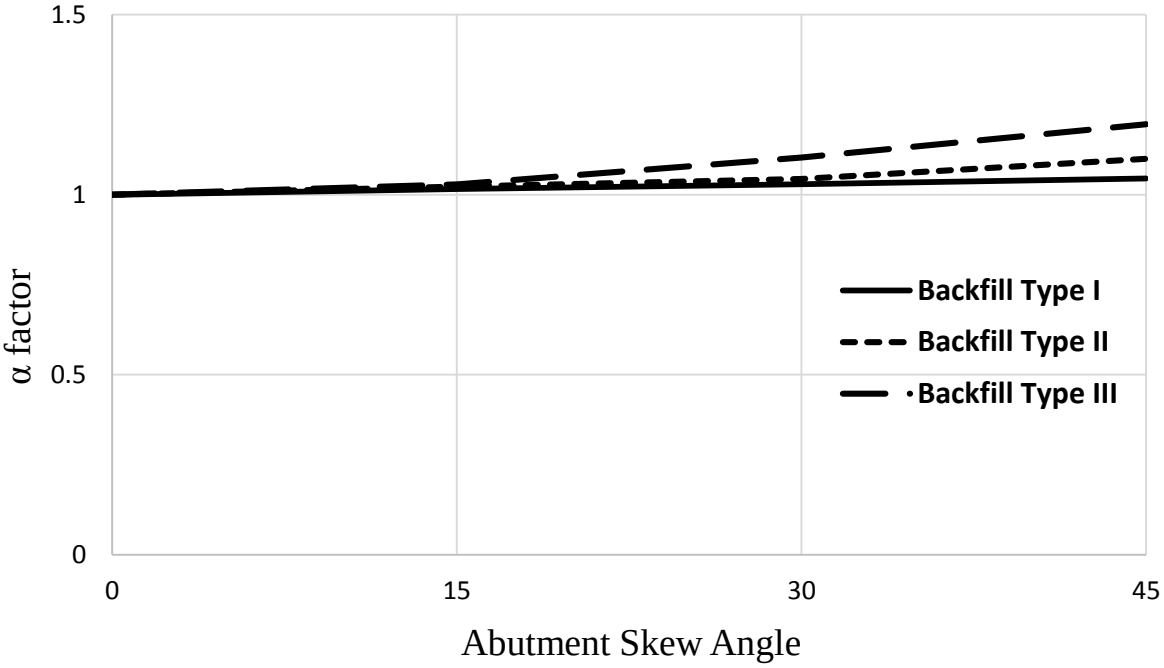

Figure 3- 16: Comparison of α factor in Bridge C with three representative GHFD backfill models (Soil Category I to III) and ductile shear key

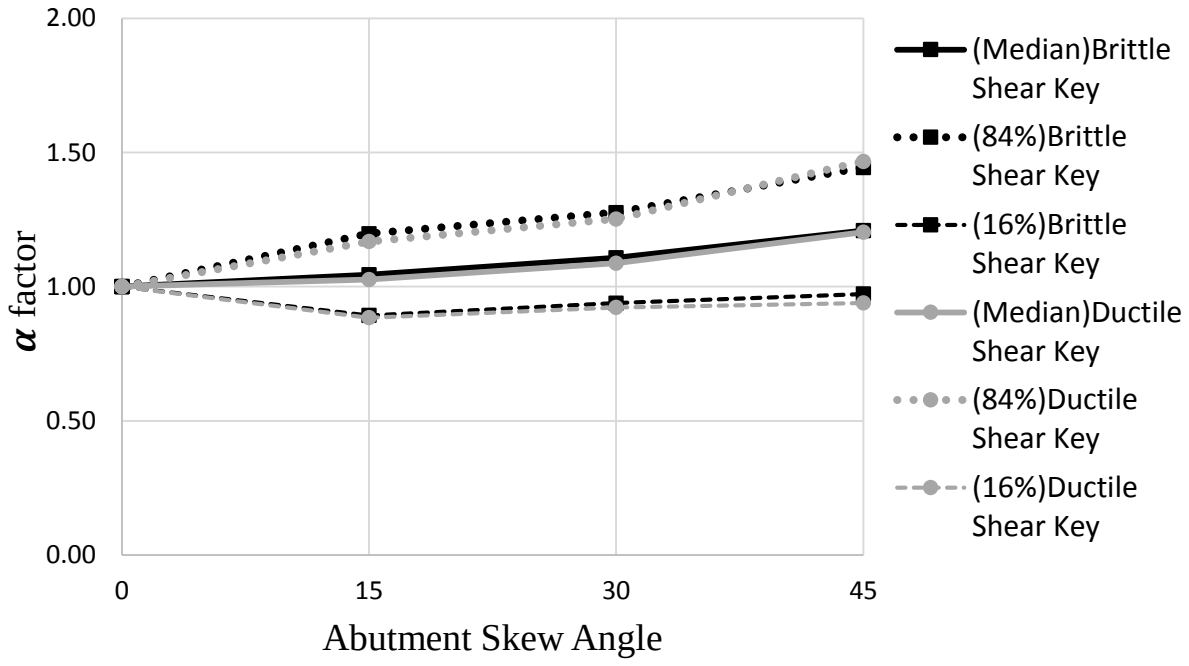

Figure 3- 17: Comparison of α factor in Bridge B with brittle and ductile shear key and category I GHFD backfill model

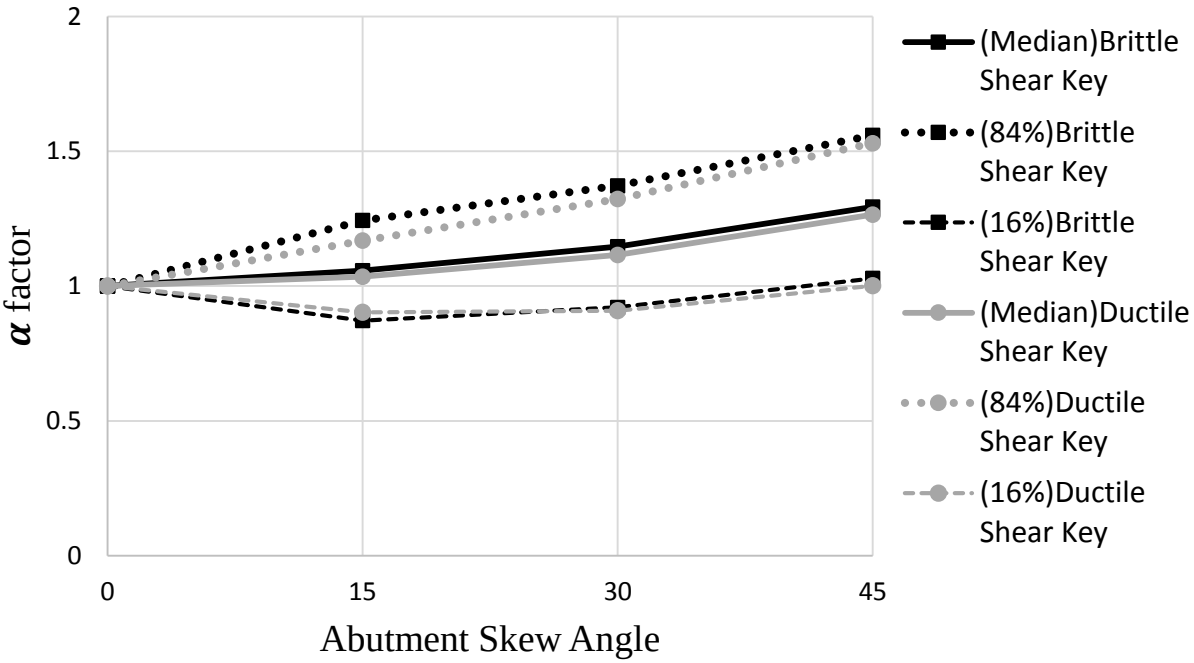

Figure 3- 18: Comparison of α factor in Bridge B with brittle and ductile shear key and category II GHFD backfill model

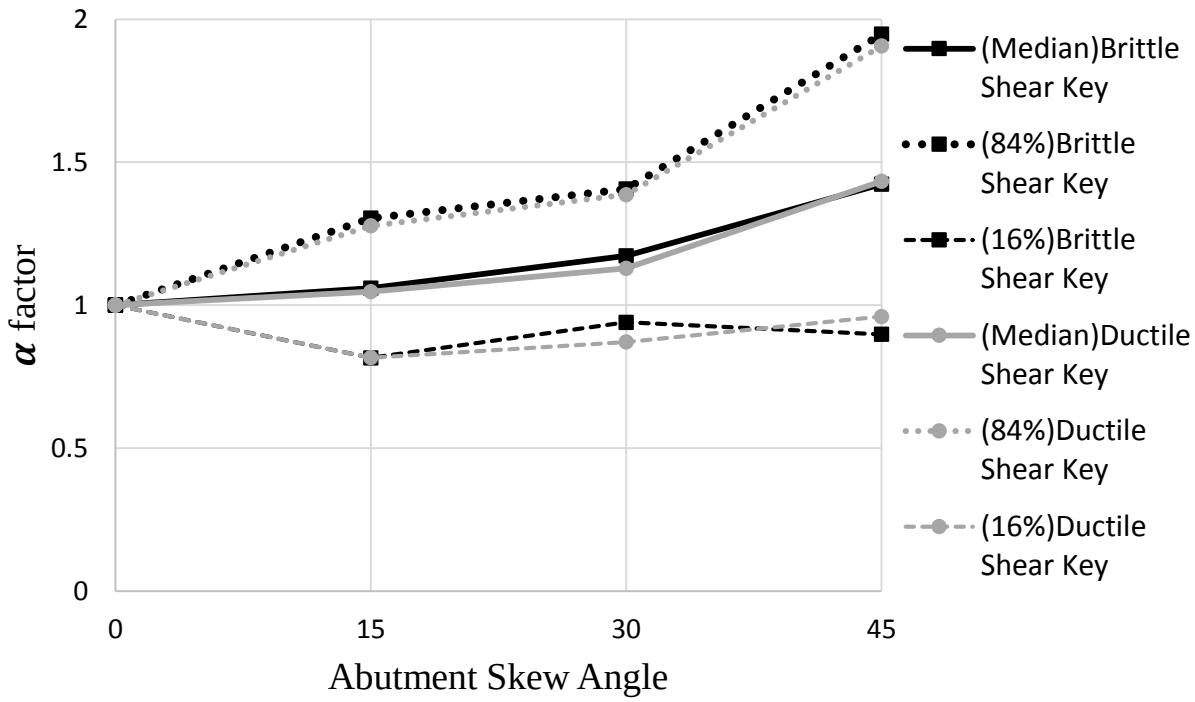

Figure 3- 9: Comparison of $\boldsymbol{\alpha}$ factor in Bridge B with brittle and ductile shear key and category III GHFD backfill model

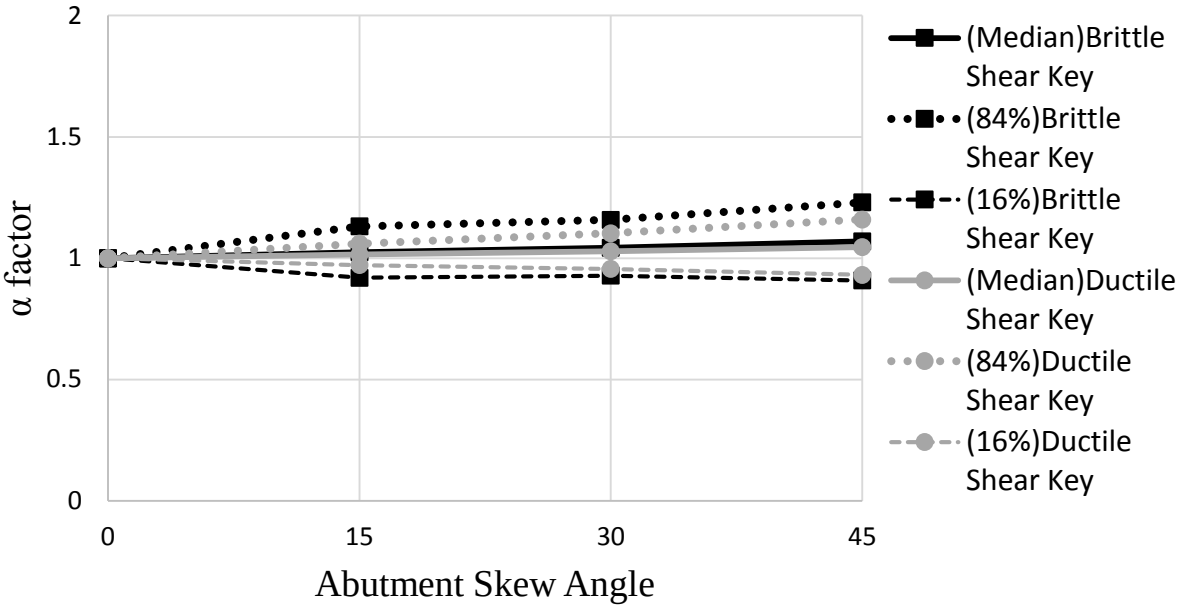

Figure 3- 10: Comparison of α factor in Bridge C with brittle and ductile shear key and category I GHFD backfill model

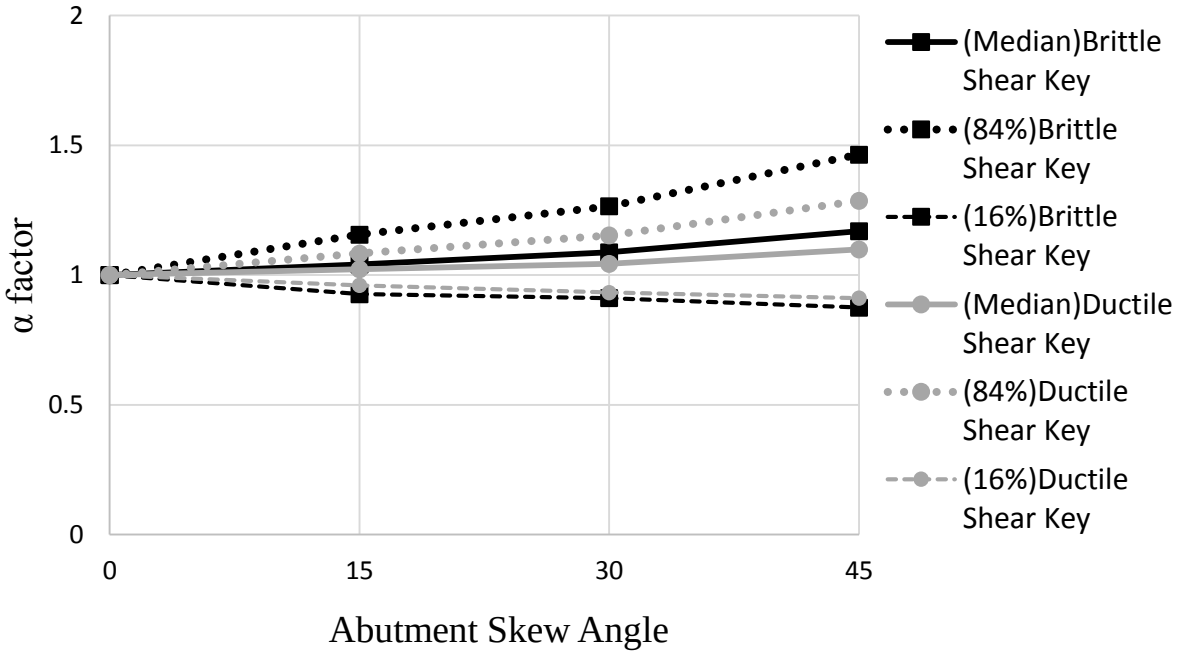

Figure 3- 11: Comparison of α factor in Bridge C with brittle and ductile shear key and category II GHFD backfill model

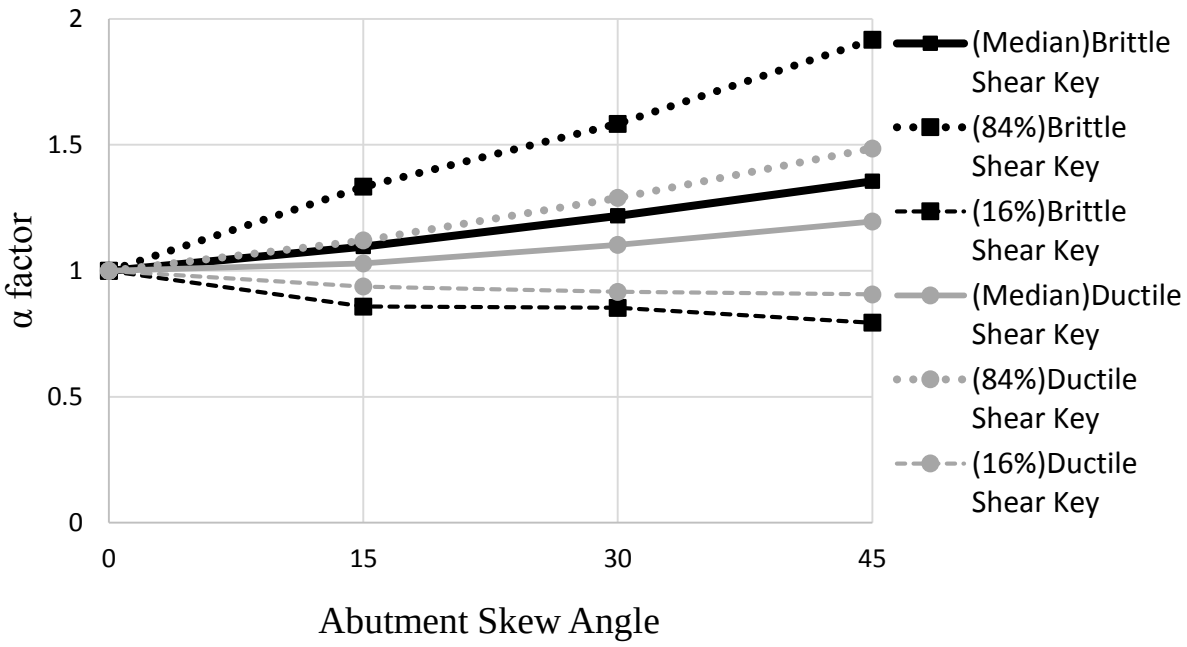

Figure 3- 12: Comparison of α factor in Bridge C with brittle and ductile shear key and category III GHFD backfill model

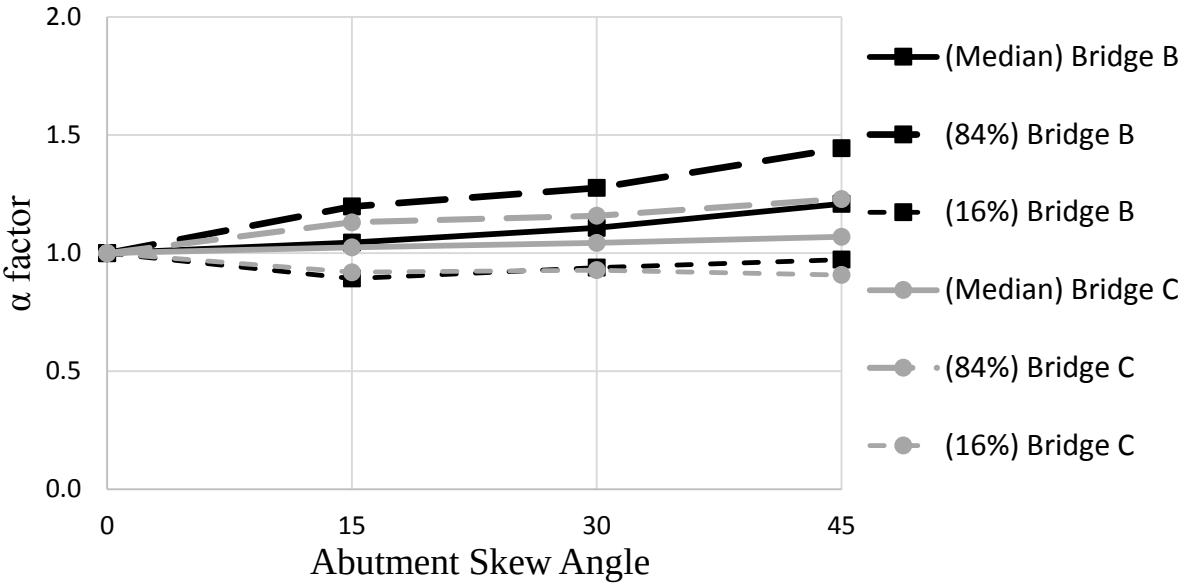

Figure 3- 13: Comparison of α factor in Bridge C and Bridge B, both with brittle shear key and category I GHFD backfill model

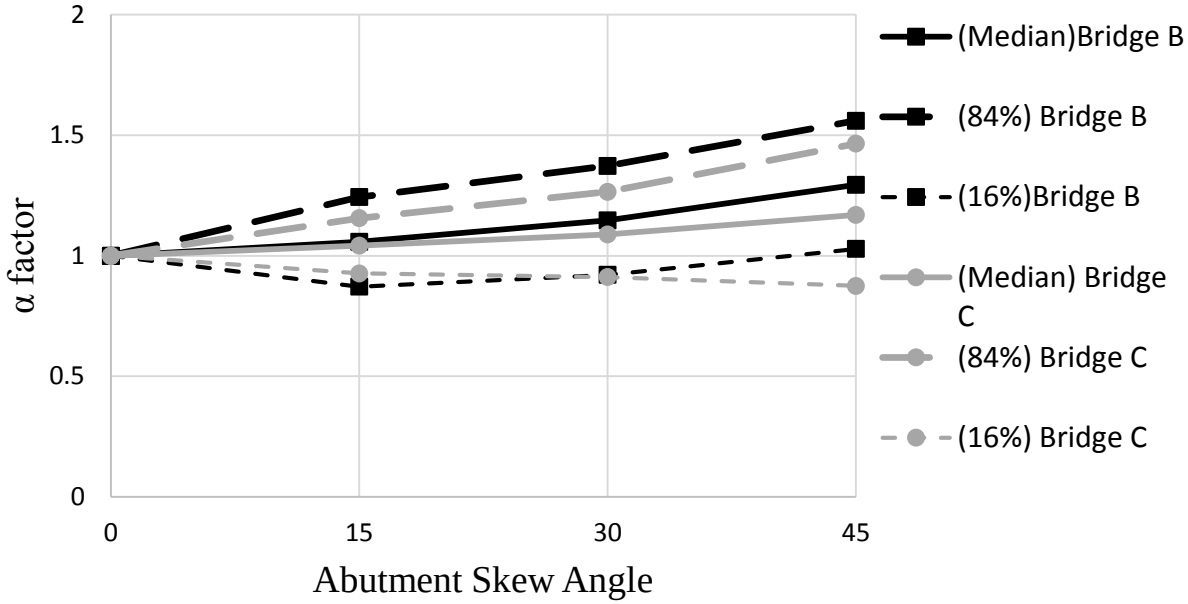

Figure 3- 14: Comparison of α factor in Bridge C and Bridge B, both with brittle shear key and category II GHFD backfill model

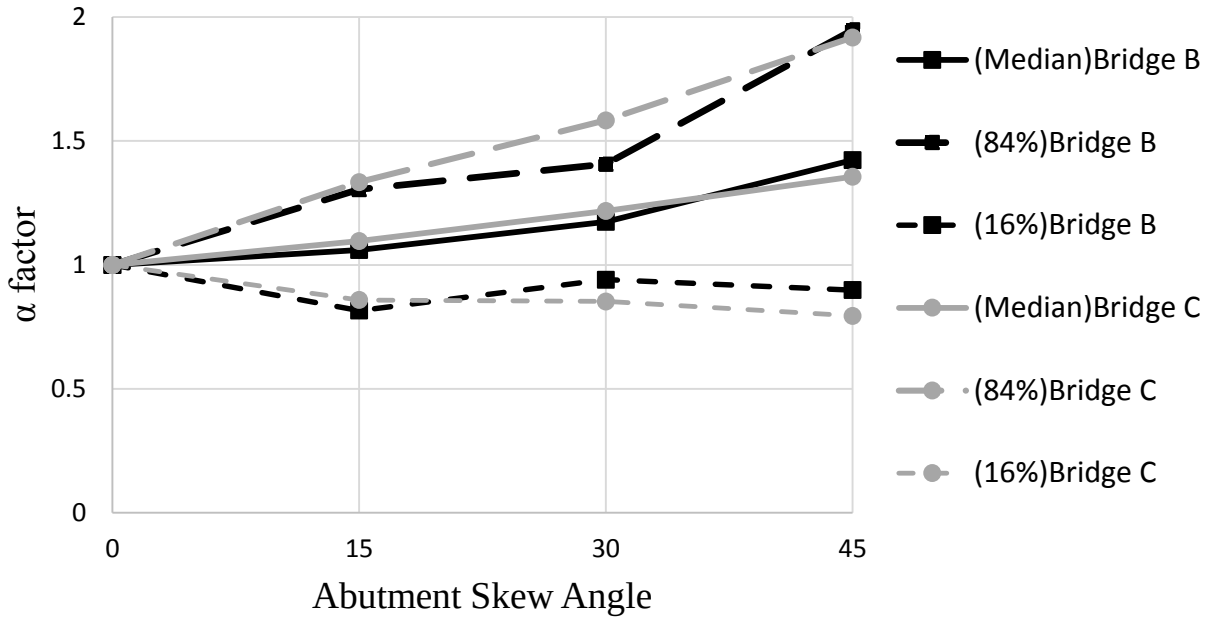

Figure 3- 15: Comparison of α factor in Bridge C and Bridge B, both with brittle shear key and category III GHFD backfill model

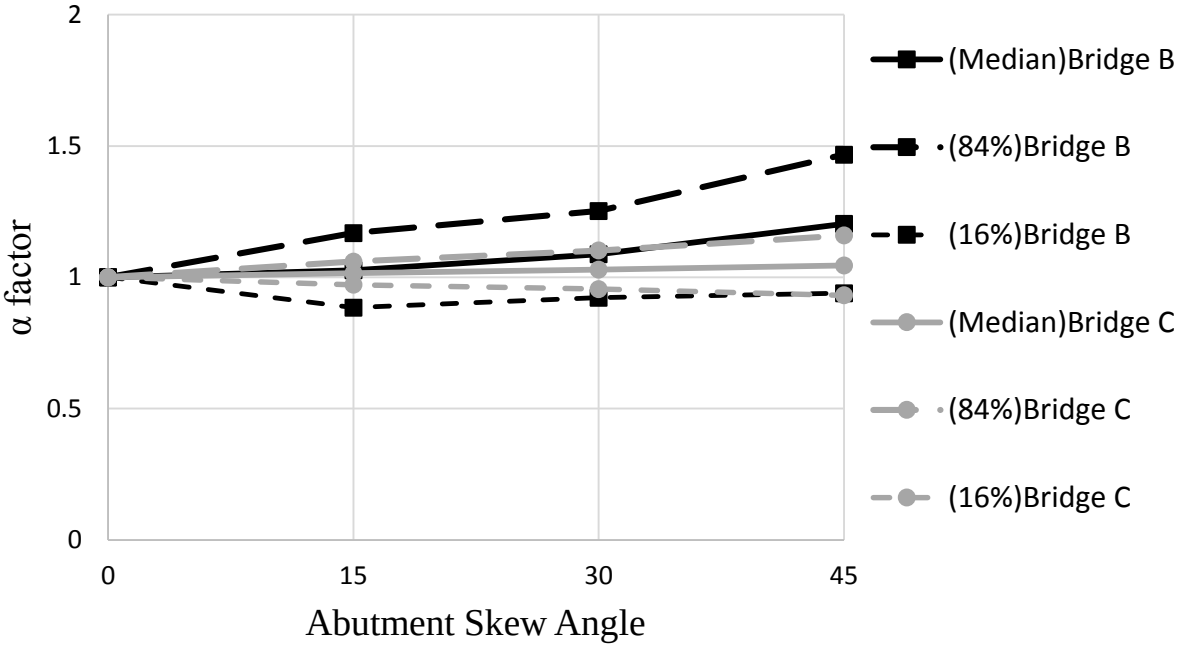

Figure 3- 16: Comparison of α factor in Bridge C and Bridge B, both with Ductile shear key and category I GHFD backfill mode

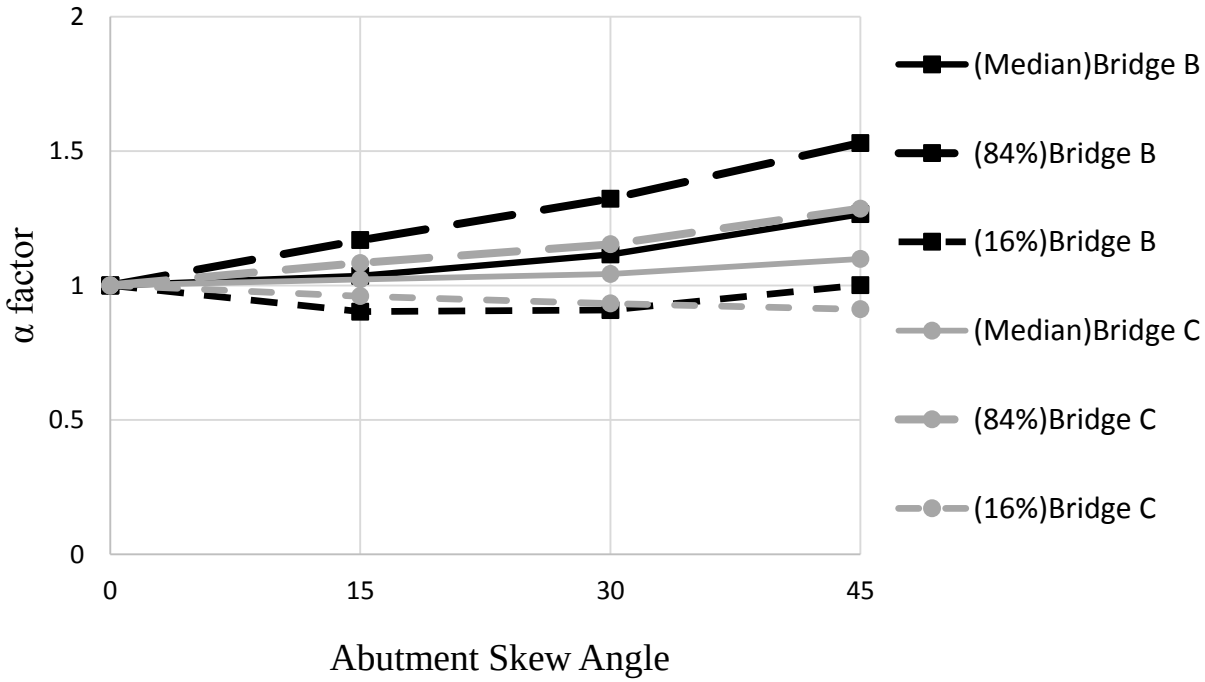

Figure 3- 17: Comparison of α factor in Bridge C and Bridge B, both with Ductile shear key and category II GHFD backfill model

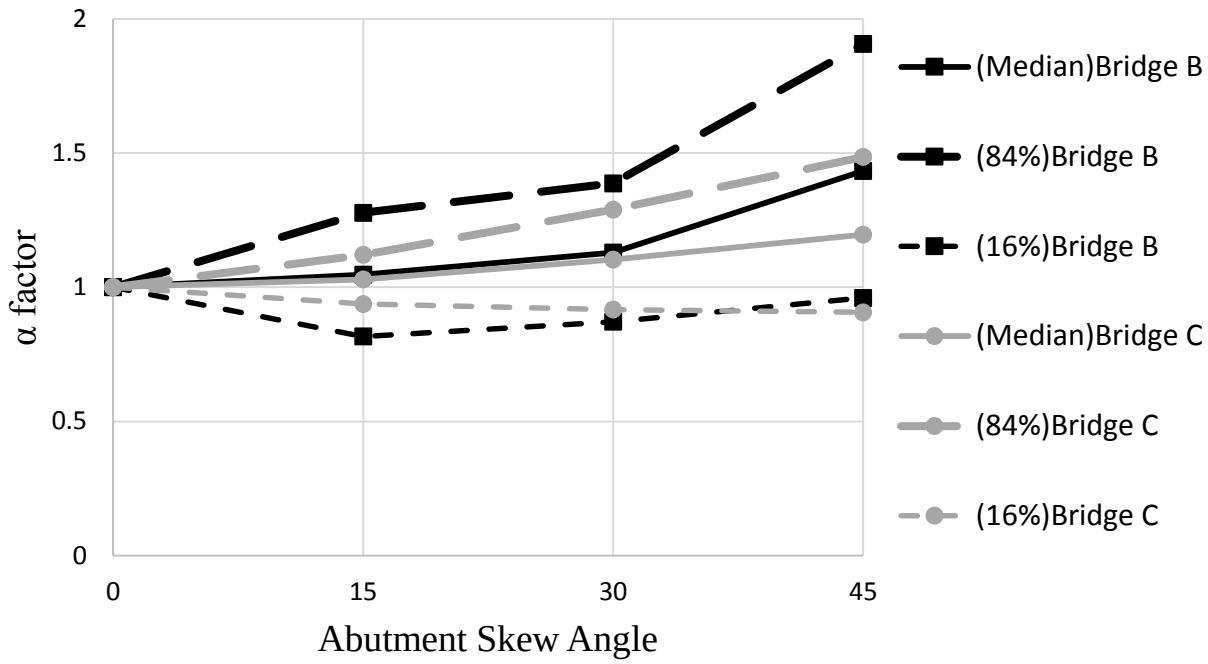

Figure 3- 18: Comparison of α factor in Bridge C and Bridge B, both with Ductile shear key and category III GHFD backfill model

Chapter 4

Conclusion and Recommendation for Future Work

4.1 Overview

This study was conducted to compare the behavior of a two-span and a multi-span skewed bridges. α,comparison parameter**,** is proposed in this research to assess the ductility demand of different bridges more efficiently. Two 3D analytical models were used as the bridge matrix for the assessment, and they were generated from two existing bridges in California. In total, 29¸760 number of response-history analysis was performed with a set of 40 pulse-like ground motions.

4.2 Skewed Bridge Modeling Technique

The main focus of the modeling work is on two components: abutment and column-bents. These components dominate the global seismic response of the bridges. The analytical models are based on the spine-line models. Five nonlinear springs attached to a rigid element represent the longitudinal response. For the transverse response, shear keys are simulated using strut-and-tie and sliding shear friction models.

4.3 Sensitivity of Bridge Response Parameters to Variation in Bridge Geometrical Properties

It was concluded that the shear key strength and backfill passive resistance force have a significant impact on the global response of skewed bridges. For comparing the ductility demand

of bridges, their span length and the rotational stiffness of the columns and bents altogether should be investigated.

The trends observed in this study are summerised as follows:

- Ductility demand in a bridge grows as the abutment skew angle increases and the backfill soil behind the abutment becomes more cohesive.
- Shear key ductility has more effect on the global behavior of longer bridges.
- Increasing the number of bents reduces the rotational and translational movement of deck substantially.

4.4 Recommendation for Future Work

The dissertation studied the behavior of two types of bridges and compared their ductility demands. The latest techniques were employed for analytical modeling of the bridges and a parameter to compare the ductility demand of bridges is proposed. For continuing the presented work, the following research topics are recommended:

1. LSH model is compared with GHFD model as a simple closed-form relationship for lateral response of abutment backwalls with uniform backfill. A further study is needed to obtain a more accurate closed-form relationship for the response of the non-skewed abutment backfill.

2. For reducing the backfill passive resistance force when the abutment is skewed, the method proposed by Omrani et al.(2016) is implemented in this study. The method focuses on the translational movement of the deck to calculate the non-uniform

reduction factor for part of the backfill passive force. A study on the effect of the rotational movement of the deck on the backfill resistance force when the abutment is skewed is recommended.

3. It is customary to model a bridge's deck with a spine-line. However, application of the technique for simulating a bridge with odd number of columns in a bent can be troublesome. In this research, the issue for modeling the three-span bridge which has three columns in each bent was solved using a technique explained in the Component Modeling section. The solution in this study is checked by modeling the bridge in SAP 2000. However, a more study is needed to find a general method for modeling the type of bridges in Opensees using spine-line model.

References

EERI (1991). “Costa Rica Reconnaissance Report.” Earthquake Spectra, Special Suppl. to Vol. 7, 127 pp.

EERI (1995). “Northridge Earthquake Reconnaissance Report.” Earthquake Spectra, Special Suppl. to Vol. 7, 127 pp.

Iwasaki, T. Penzien, J., and Clough, R.W.(1972). “ Liturature Survay-Seismic Effects on Highway Bridges.” Earthquake Engineering Report No. 72-11, University of California, Berkeley, CA.

Jennings. P. C.,(editor), Housner, G. W., Hudson, D. E., Trifunac. M. D., Fraizer, G. A., Wood, J. H., Scott, R. F., Iwan, W. D., and Brady, A. G. (1971). “Engineering Features of San Fernando Earthquake of February 9 , 1971.” Report no. EERL 71-02, California Institute of Technology, Pasadena.

Kawashima, K, Unjoh, S.,Hoshikuma,J., and Kosa,K (2010).”Damage of Transportation Facility due to 2010 Chile Earthquake (April 5, 2010). Bridge Team Dispatched by Japan Society of Civil Engineerings.”

Yashinsky, M., Oviedo, R., Ashford, S. A., Fragier-Gabaldon, L., and Hube, M.(2010) “Performance of Highway and Railway Structures During February 27 , 2010 Maule Chile Earthquake.” EERI/PEER.FHWA Bridge Team Report,.

McKenna, F., Fenves, G. L., and Filippou, F. C., and Mazzoni, S. (2000). “Open System for Earthquake Engineering Simulation.” University of California, Berkeley, CA.

California Department of Transportation (Caltrans). (2013). “Caltrans Seismic Design Criteria, Version 1.7.” California Department of Transportation, Sacramento, CA.

Nielson, B. G. (2005). “Analytical fragility curves for highway bridges in moderate seismic zones.” Ph.D. Dissertation, Georgina Institute of Technology, Atlanta, GA.

Nielson, B. G., and DesRoches, R. (2006). “Influence of modeling assumptions on the seismic response of multi-span simply supported steel girder bridges in moderate seismic zones.” Engineering structures, 28(8), 1083–1092.

Aviram, A., Mackie, K. R., and Stojadinovic, B. (2008). “Effect of abutment modeling on the seismic response of bridge structures.” Earthquake Engineering and Engineering Vibration, 7(4), 395–402.

Kaviani, P., Zareian, F. and Taciroglu, E. (2012) “Seismic behavior of reinforced concrete bridges with skew-angled seat-type abutments.” Engineering Structures, 45, 137–150.

Bozorgzadeh, A., Megally, S., Restrepo, J., and Ashford, S. A. (2006) “Capacity evaluation of exterior sacrificial shear keys of bridge abutments.” Bridge Engineering, 11(5), 555-565.

Bozorgzadeh, A., Megally, S., and Restrepo, J. (2007) “Seismic response of sacrificial exterior shear keys in bridge abutments: Recommended design and construction details.” Report No. SSRP–04/14, University of California, San Diego, CA.

Megally, S., Silva, P. F., and Seible, F. (2001). “Seismic response of sacrificial shear keys in bridge abutments.” Report No. SSRP–2001/23, University of California, San Diego, CA.

Huo, Y. (2011). “Seismic response Assessment and improvement of highway bridges using fragility function method.” Ph.D. Dissertation, University of California, Los Angeles, CA.

Huo, Y., and Zhang, J. (2012). “Effects of pounding and skewness on seismic responses of typical multispan highway bridges using the fragility function method.” Journal of Bridge Engineering, 18(6), 499–515.

Shamsabadi, A., Yan, L., and Martin, G. R. (2004). “Three dimensional nonlinear seismic soil-foundation-structure interaction analysis of a skewed bridge considering near fault effects.” Proc., US-Turkey Soil-Structural Interaction Workshop, Turkey.

Buckle, I. G. (1994). “The Northridge, California earthquake of January 17, 1994: Performance of highway bridges.” Technical Report NCEER-94-0008, National Center for Earthquake Engineering Research, State University of New York, Buffalo, NY.

Kawashima, K., Unjoh, S., Hoshikuma, J. I., and Kosa, K. (2011). “Damage of bridges due to the 2010 Maule, Chile, earthquake.” Journal of Earthquake Engineering, 15(7), 1036–1068.

Shamsabadi, A., Kapuskar, M. (2006). “Nonlinear seismic soil-abutment-structure interaction analysis of skewed bridges.” Proc., 5th National Seismic conference on bridges and highways, San Francisco, CA.

Rollins, K. M., and Jessee, S. J. (2012). “Passive force-deflection curves for skewed abutments.” Journal of Bridge Engineering, 18(10), 1086–1094.

Marsh, A. K., Rollins, K. M., Franke, B., Smith, J., and Palmer, K. (2013). “Passive force-deflection behavior for 0° and 30° skewed abutments.” Transportation Research Record: Journal of the Transportation Research Board, 2363(1), 12–20.

Zakeri, B., Padgett, J. E., and Amiri, G. G. (2013). “Fragility analysis of skewed single frame concrete box girder bridges.” Journal of Performance of Constructed Facilities, 28(3), 571–582.

Zhang, J. and Makris, N. (2002) “Kinematic response functions and dynamic stiffnesses of bridge embankments," Earthquake Engineering and Structural Dynamics, 31(11), 1933–1966.

Wakefield R. R., Nazmy, A. S., and Billington, D. P. 1991. “Analysis of Seismic Failure in Skew RC Bridge,” *Journal of Structural Engineering (ASCE)*, 117(3): 972-986.

Hansen , R. J., Nawy, E. G., and Shah, J. M.(1961). “Response of Concrete shear keys to dynamic loading.” ACI J.,32(11), 1475-1490

Buyukozturk, O., Bakkhoum, M. M., and Micheal Beattie, S. (1990). “ Shear Behavior of Joints in precast concrete segmental bridges.” J. Struct. Eng., 116(12), 3380-3401.

Silva, P. F., Megally, S., and Seible, F.(2003). “Seismic Performance of Sacrificial interior shear keys.” ACI Mater. J., 100(2), 177-187

Anderson, A. R. (1960). “ Composite designs in precast and cast-in-place concrete.” Progressive Architecture, September, 172-179.

Mast, R. F. (1968). “Auxiliary reinforcement in concrete connections.” J. Struct. Div. ASCE, 94(ST6), 1485-1504

Mattock, A. H., and Hawkions, N. M.(1972). “Research on shear transfer in reinforced concrete.” PCI J., 17(2), 55-75.

Mattock, A. H. (1974). " Shear transfer in concrete having reinforcement at an angle to the shear plane." Shear in Reinforced Concrete, ACI Special Publication 42, 17-42.

Mattock, A. H. (1981). "Cyclic shear transfer and type of interface." J. Struct. Div. ASCE, 107(ST10), 1945-1964.

Mattock, A. H. (1975). " Shear transfer in reinforced concrete with moment or torsion acting across the shear plane." PCI J., 20(4), 76-93.

Paulay, T., Park, R., and Phillips, M. H.(1974). "Horizontal construction joints in cast in place reinforced concrete." Shear in Reinforced Concrete, ACI Special Publication 42, 559-616.

Walraven, J. C., Frenay, J., and Pruijssers, A.(1987). "Influence of concrete strength and load history on the shear friction capacity of concrete members." PCI J., 32(1), 66-83.

Tassios, T. P., and Vintzeleeou, E. N. (1987). "Concrete-to-concrete friction." J.Struct. Eng., 113(4), 832-849

CSI (2014). "SAP 2000-Linear and Nonlinear Static and Dynamic Analysis and Design of Three-Dimensional Structures: Basic Analysis Reference Manual." Computer and Structures, Inc.

Mander, J. B., Priestley, M. J. N., and Park, R. (1988). "Theoretical Stress-Strain Model for Confined Concrete." Journal of Structural Engineering(ASCE), 114(8): 1804-1825.

Priestley, M. J. N., Calvi, G. M., and Seisble, F. (1996). Seismic Design and Retrofit of Bridges, John Wiley & Sons, NY.

Khalili-Tehrani, P., Taciroglu E., and Shamsabadi, A. (2010). "Backbone curves for passive lateral response of walls with homogeneous backfills." Soil-Foundation-Structure Interaction, R.P. Orense, N. Chouw, N., and M. J. Pender, eds., University of Auckland, New Zealand, vol. 2, 149–154.

Shamsabadi, A., Khalili-Tehrani, P., Stewart, J. P., and Taciroglu, E. (2010). "Validated simulation models for lateral response of bridge abutments with typical backfills." Journal of Bridge Engineering, 15(3), 302-311.

Shamsabadi, A., Rollins, K. M., and Kapuskar, M. (2007). "Nonlinear soil–abutment–bridge structure interaction for seismic performance-based design." Journal of Geotechnical and Geoenvironmental Engineering, 133(6), 707-720.

Wilson, J. C. and Tan, B. S. (1990). "Bridge Abutment: Formulation of Simple Model for Earthquake Response Analysis." Journal of Engineering Mechanics (ASCE), 116(8): 1828-1837.

Duncan, J. M., and Chang, C.-Y. (1970). "Nonlinear analysis of stress and strain in soils." J.Soil Mech. And Found. Div., 96(5), 1629-1653.

James, R. G., and Bransby, P. L. (1971). "Experimental and theoretical investigation of a passive earth pressure problem." Geotechnique, 20(1), 17-36.

Earth Mechanics, INC. (2005). "Field investigation report for abutment backfill characterization." Report No. SSRP-05/02, University of California, San Diego, CA.

Omrani et al. (in progress). "Variability in the Predicted Seismic Performance of a Typical Seat -type Bridge Due to Epistemic Uncertainties in its Abutment Backfill and Shear-key Models"